

Review

Fundamentals, rational catalyst design,
and remaining challenges in electrochemical
NO_x reduction reactionAngga Hermawan,^{1,*} Vani Novita Alviani,² Wibisono,³ and Zhi Wei Seh^{4,*}

SUMMARY

Nitrogen oxides (NO_x) emissions carry pernicious consequences on air quality and human health, prompting an upsurge of interest in eliminating them from the atmosphere. The electrochemical NO_x reduction reaction (NO_xRR) is among the promising techniques for NO_x removal and potential conversion into valuable chemical feedstock with high conversion efficiency while benefiting energy conservation. However, developing efficient and stable electrocatalysts for NO_xRR remains an arduous challenge. This review provides a comprehensive survey of recent advancements in NO_xRR, encompassing the underlying fundamentals of the reaction mechanism and rationale behind the design of electrocatalysts using computational modeling and experimental efforts. The potential utilization of NO_xRR in a Zn-NO_x battery is also explored as a proof of concept for concurrent NO_x abatement, NH₃ synthesis, and decarbonizing energy generation. Despite significant strides in this domain, several hurdles still need to be resolved in developing efficient and long-lasting electrocatalysts for NO_x reduction. These possible means are necessary to augment the catalytic activity and electrocatalyst selectivity and surmount the challenges of catalyst deactivation and corrosion. Furthermore, sustained research and development of NO_xRR could offer a promising solution to the urgent issue of NO_x pollution, culminating in a cleaner and healthier environment.

INTRODUCTION

Air pollution remains a grave concern that plagues the world, as millions of individuals succumb to premature deaths each year due to inhalation of toxic air.¹ The World Health Organization (WHO) has reported that an estimated 7 million people meet their untimely demise yearly due to air pollution, with over 90% of these fatalities transpiring in low- and middle-income countries.^{2,3} While the sources of air pollution vary, they predominantly stem from industrial activities, transportation, power generation, and residential heating and cooking.² Particulate matter (PM), nitrogen oxides (NO_x), sulfur oxides (SO_x), and volatile organic compounds (VOCs) rank among the most noxious air pollutants, imperiling human health and the environment.^{4,5}

NO_x is one of the most significant contributors to air pollution, and it has been linked to respiratory and cardiovascular diseases, lung cancer, and stroke.^{4–6} The impact of air pollution particularly concerns vulnerable groups such as children, elderly individuals, and those with underlying health conditions.⁷ Moreover, it has significant environmental consequences, as likely as acid rain, ozone depletion, and climate change. In the US, transportation is responsible for the largest share of NO_x emissions, contributing approximately 36% of the total emissions in 2017.⁸ Meanwhile, power generation and industrial activities are responsible for 23% and 17% of total NO_x emissions, respectively.^{9,10} Globally, the International Energy Agency (IEA) estimated that in 2020, NO_x emissions from the power sector and transportation reached 14.6 million and 13.7 million metric tons, respectively. As such, developing effective strategies to reduce NO_x emissions from these sources is crucial. Governments and various institutions across the globe are making concerted efforts to curb NO_x emissions by enforcing more stringent regulations on emissions from automobiles and power plants while encouraging the adoption of cleaner energy technologies.^{10–12} Nevertheless, NO_x emissions continue to substantially threaten air quality and the health of living beings, calling for more

¹Research Center for Advanced Materials, National Research and Innovation Agency (BRIN), South Tangerang City, Banten 15314, Indonesia

²Graduate School of Environmental Studies, Tohoku University, Sendai 9808579, Japan

³Research Center for Radiation Detection and Nuclear Analysis Technology, National Research and Innovation Agency (BRIN), South Tangerang City, Banten 15314, Indonesia

⁴Institute of Materials Research and Engineering (IMRE), Agency for Science, Technology and Research (A*STAR), 2 Fusionopolis Way, Innovis #08-03, Singapore 138634, Republic of Singapore

*Correspondence: angga.hermawan@brin.go.id (A.H.), sehzw@imre.a-star.edu.sg (Z.W.S.)

<https://doi.org/10.1016/j.isci.2023.107410>



intensive efforts to mitigate their impact on human health and the environment.^{9,13} Researchers have explored various methods and technologies to obviate the deleterious effects of NO_x pollution and abate NO_x emissions. Among them, selective catalytic reduction (SCR) is the most widely used in stationary applications, selective noncatalytic reduction (SNCR) is applied in specific situations, and other technologies are still being explored (e.g., electrochemical NO_x reduction).

NH₃ is a highly sought-after chemical compound for its role as a crucial feedstock in the production of fertilizers.¹⁴ This is due to its nitrogen content, which is essential for the growth of plants. As a matter of fact, it is the most widely utilized chemical worldwide for fertilizer production.^{14,15} The current global demand for NH₃ as a chemical feedstock exceeds 150 million tons per year, and this demand is expected to grow in the coming years in response to the increasing need for food and enhanced crop yields.¹⁶ In addition to global agriculture for nitrogen-based fertilizer use, a solid incentive to deploy NH₃ for chemical and energy industries is expected to grow at different scales. Due to its relatively high H₂ content, NH₃ can be directly combusted as likely end-use H₂ or used as a feedstock in manufacturing. Given the anticipated future demand, alternative NH₃ synthesis is an emerging area to pursue. At present, the Haber-Bosch process, first developed in the early 20th century, is the predominant method used to produce NH₃. This process entails reacting highly purified N₂ gas with H₂ gas obtained from natural gas or other hydrocarbons in the presence of a catalyst under high pressure (10–30 MPa) and temperature (400–500°C).^{17–19} The resultant product, NH₃, is subsequently collected and purified. However, this process is not without its flaws, such as its considerable energy consumption and emission of greenhouse gases like CO₂ during production to perform the reaction properly; the best available techniques consume energy of about 27.4–31.8 GJ t_{NH₃}⁻¹.²⁰ The development of more sustainable methods for NH₃ production is, therefore, crucial to ensure a reliable and sustainable supply of this essential chemical feedstock.

The electrochemical reduction of NO_x, hereafter known as NO_xRR, presents an innovative and environmentally friendly opportunity for the elimination of NO_x pollutants and sustainable NH₃ production.²¹ This technology can be performed at ambient pressure and room temperature, making it an ideal approach for scaling up and industrial applications.²² The lower bond energy and polar nature of NO compared to N₂ (N=O 607 kJ mol⁻¹, N≡N 941 kJ mol⁻¹ at 25°C) results in lower activation energy and more energy-efficient electrolysis than its nitrogen reduction reaction (NRR) counterpart.^{23–25} Moreover, the technology has demonstrated high selectivity toward NH₃ production and provides precise control over reaction conditions, allowing for a finely tuned NH₃ production rate. It can also be powered using renewable sources of electricity, such as photovoltaic (PV) technology, which enhances an additional layer of environmental friendliness, making it a reliable and sustainable solution for mitigating NO_x emissions and reducing the overall carbon footprint of the process.²¹ The integration of these technologies also has immense potential for reducing NO_x emissions while promoting sustainable development. The deployment of such systems can also contribute to overall grid stability and reduce reliance on traditional energy sources, thereby enabling the use of renewable energy.

The conversion of NO_x through electrochemical reduction is a complicated process that includes several reactions and intermediate steps involving the transfer of both protons and electrons, leading to the formation of stable end products.²⁶ However, this process is often fraught with challenges as it tends to produce residual nitrogen-containing compounds such as NO₂, N₂, N₂O, and N₂H₄, which not only impede the overall efficiency of the reaction but also contribute to environmental pollution.^{23,27–31} The slow reaction kinetics resulting from gaseous NO's low solubility in aqueous electrolytes and the concurrent hydrogen evolution reaction (HER) pose fundamental obstacles to NO_xRR.^{29,32} Regrettably, electrocatalytic NO_xRR techniques suffer from relatively low NH₃ yield and selectivity. Moreover, the design of high-performing and durable electrocatalysts for NO_xRR still presents significant challenges. Catalyst deactivation, corrosion, and electrode fouling are other issues that can reduce the efficiency and lifespan of electrocatalysts, especially in corrosive environments and highly acidic electrolytes.^{31,33} Despite the intricate kinetics and complexity involved in the electrochemical reduction of NO_x, recent years have witnessed significant strides in the development of efficient and cost-effective electrochemical NO_xRR systems. Numerous electrocatalytic materials, including single-atom catalysts (SACs), metal oxides, metal sulfides, and metal phosphides, have been computationally and experimentally explored for their ability to catalyze this reaction.^{23,24,32,34,35} Given the rapid acceleration of research progress in the field of NO_xRR, a comprehensive review that provides a panoramic overview of the current state of research and directs future efforts is imperative yet nonexistent to our knowledge. Thus, this review aims to present an up-to-date and comprehensive discussion, spanning from elucidating the underlying mechanisms of the NO_xRR to conducting a thorough theoretical screening through computational simulations. We also

summarize the cutting-edge developments in various electrocatalysts and gas diffusion layers (GDE) for NO_xRR for the scale-up study. More importantly, we highlight the proof-of-concept of the Zn-NO_x battery using NO_xRR electrocatalysts as the cathode materials. It is more attractive to develop the Zn-NO_x battery as a promising “3-in-1” strategy: reduce NO_x emission, produce NH₃, and generate electrical energy. Finally, we examine the current challenges and provide a perspective on future efforts to optimize electrochemical NO_xRR. We anticipate that this review will inspire significant research and essential advancements in the field of electrocatalysts for emerging NO_xRR.

EXISTING TECHNOLOGIES FOR NO_x MITIGATION

Selective catalytic reduction

Selective catalytic reduction (SCR) is the most widespread state-of-the-art technology for NO_x mitigation and is deemed the most efficacious technology that harnesses a catalyst to transmute NO_x into nitrogen (N₂) and water vapor (H₂O) at an appropriate temperature range of 200°C–400°C, resulting in a NO_x emissions decline of up to 90%.^{36–38} A reductant, commonly anhydrous ammonia (NH₃), aqueous ammonia (NH₄OH), or a urea (CO(NH₂)₂) solution, is infused into a stream of flue or exhaust gas and is reacted upon a catalyst.^{39–42} As the reaction progresses, N₂ and carbon dioxide (CO₂) are generated, if urea is utilized. SCR systems necessitate a dependable source of NH₃ or other reducing agents, which might entail supplementary expenses for conveyance and storage, causing energy consumption.^{37,42} Furthermore, the implementation of SCR catalysts is frequently hindered by the inclusion of precious metals, such as Pt, Pd, Ir, or Ru, which restrains its usage in industrial scale applications.³⁸ An unsatisfactory design or maintenance of SCR systems may cause unreacted NH₃ to be vented into the atmosphere, posing a significant hazard to public health and the environment.⁴³ The catalyst employed in SCR systems may be contaminated over time due to contact with pollutants, such as sulfur, reducing its potency. Therefore, although SCR technology is remarkably effective in mitigating NO_x emissions, it is crucial to assess its advantages versus the costs and potential shortcomings.

Selective non-catalytic reduction

Flue gases are often generated in the industrial processes with noticeable particles and reactive volatiles, which lead to the deactivation of a bulky unit of catalyst beds over time, raising overall operating and capital costs.⁴⁴ With the long-life expectancies of industrial plants, technology to mitigate their pollution ought to be retrofitted within a lifetime.⁴⁵ When the catalysts are found non-viable for NO_x mitigation, the SNCR process is one of the relevant options.⁴⁶ In the SNCR, NO_x is reduced to N₂ with NH₃ or, alternatively, CO(NH₂)₂, ammonia salts, or cyanuric acid at high temperatures ranging from 900°C to 1000°C.⁴⁶ Unlike SCR, the SNCR takes place without the need for a catalyst. The reported SNCR efficiencies are 30–70% depending upon several factors, including temperature, NO_x level, reagent-flue gas mixing, NH₃-NO_x ratio, and reaction time, but efficiencies as high as 80% are also achievable.⁴⁷ SNCR has fewer capital costs than SCR as the simplicity of the process only requires reagent storage and injection equipment, there is no need for a catalytic bed, and it is easier to retrofit, which is likely suited to be adopted by major industries in developing countries.⁴⁷ Operating costs, however, are comparable to the SCR. Some issues correspond with the unreacted NH₃ (otherwise known as NH₃ slips), formation of NH₄HSO₄, and N₂O.⁴⁷ The NH₃ slip and N₂O formation can be resolved with careful control of operating parameters. The NH₄HSO₄ may corrode and plug equipment.⁴⁷ Despite the prevalence of the SNCR process thus far, some general disadvantages make the technology less appealing in meeting the context of stringent emission standards and, therefore, developing alternatives to mitigate NO_x emissions is of great interest.

FUNDAMENTALS OF ELECTROCATALYTIC NO_x REDUCTION REACTION MECHANISM IN AQUEOUS ELECTROLYTES

The previously reported NO_x mitigation technologies have been increasingly under pressure because of various specific challenges. Alternative technologies have been explored in an attempt to substitute or improve upon current traditional mitigation facilities. The NO_xRR is amongst prospective means that challenge the *status quo*. Although NO_xRR is still in its infant development, the prospects of this concept are promising owing to the fuel cell development for energy generation that has generally accelerated and the reported results on NO_xRR that compare favorably with solid oxide fuel cells.⁴⁸

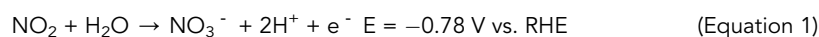
NO_x capture

To date, research on electrochemical NO_x reduction is almost exclusively performed on the benchtop scale.⁴⁹ The control and reduction of NO_x emissions usually implement particular emission control technologies and practices involving the emission treatments at the sources (e.g., industrial stacks or exhaust systems); amongst the essential considerations is therefore to capture NO_x from its source prior to NO_xRR operation in aqueous electrolytes. Adopted from the production of N₂-containing compounds from the air (so-called N₂ fixation), there are pioneering developed industrial methods reported as thermal and non-thermal plasma. A published work used thermal plasma arc discharge with a temperature >3000°C to activate air, followed by quenching with water to synthesize nitric acid. The major disadvantage of this process for N₂ fixation is definitely its higher energy requirements.^{49,50} Non-thermal plasma is rather more advantageous to generate high energy electrons with temperatures several orders of magnitudes more elevated than the surrounding gas due to an ionized gas composed of a range of species (including electrons, ions, radicals, molecular fragments) at various energy levels.⁵⁴ This process is applicable for several applications ranging from rapid synthesis to surface modification of electrode materials.^{51–53} It is likely to create high-energy species that can activate atmospheric dinitrogen molecules while keeping the reaction temperature and energy consumption for NO_x generation lower than the thermal plasmas in small-scale reactors, which are even much lower than the Haber-Bosch process.⁵⁴ According to this ground, the non-thermal plasma with much-improved rate and energy efficiency is preferable for the facile NO_x capture in the scalable NO_xRR as it was reported to be potential for NO_x fixation into ammonium at very low cell potentials whilst obtaining considerable ammonium yields and rate.⁵⁴

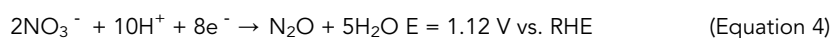
As collective efforts to mitigate NO_x pollution, NO_x capture technologies are in place as an emerging area to explore NO_x to NH₃. As the relevant studies are undergoing, novel findings that offer long-term technological and environmental benefits are open areas to fill and very much looked forward to. Being typical early stage technologies, NO_xRR may face immaturity and cost-inefficiency at its first development, but technological advancements, growing markets, and accumulated experience will undoubtedly aid its further development.

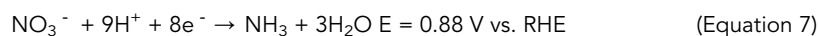
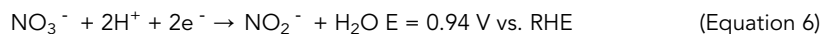
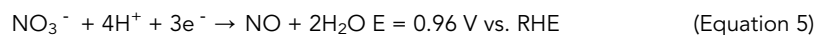
Electrocatalytic NO_x reduction reaction mechanism in aqueous electrolytes

Exploring the fundamental mechanism of electrochemical NO_x reduction is an indispensable step toward developing efficient electrocatalysts and achieving high conversion yields. However, the NO_xRR faces significant challenges due to the involvement of multiple intermediate species, making it difficult to predict the reaction pathway and the stability of the products. NO_x comprises a mixture of N₂O, NO, NO₂, N₂O₃, N₂O₄, and N₂O₅, with NO and NO₂ accounting for 90% and 5%, respectively. While most NO_x reacts easily with liquid water, NO and NO₂ exhibit low solubility in water. Consequently, the electrochemical reduction process of NO_x becomes exceedingly intricate, involving multiple proton-electron coupling reactions and the formation of stable products and intermediates. The focus is placed on the electroreduction of NO and NO₂ species to simplify the reaction. NO₂, being water-soluble, is readily transformed into nitrites (NO₂[−]) and nitrates (NO₃[−]) under reduction conditions, as indicated in Equations 1 and 2, respectively^{23,27–30}:

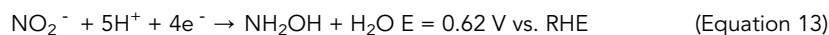
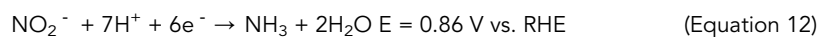
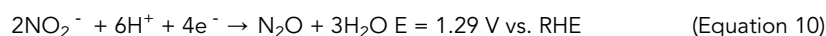
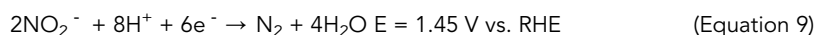


Upon further reduction of NO₃[−], a plethora of intermediates can be generated, including but not limited to NH₃, NO₂[−], hydroxylamine (NH₂OH), NO, and N₂O. The specific intermediates formed are contingent on the potential observed during electrochemical reduction, highlighting the complexity of the reaction process.

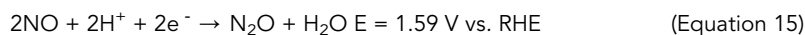




Similarly, NO_2^- reduction will proceed through the following reactions:



Amidst the plethora of electrochemical studies, several have demonstrated that NO reduction, under varying reaction conditions, tends to traverse four distinct routes:



The associative and dissociative mechanisms of NRR typically describe the formal reaction pathways of electrochemical NO_xRR . He et al.⁵⁴ utilized density functional theory (DFT) calculations with 2D transition metal borides (MBenes), such as CrB, MnB, MoB, HfB, and WB, as model catalysts to elucidate the associative and dissociative mechanisms of NO_xRR . The hydrogenation of adsorbed NO molecules on the surface of MBenes can generally follow two different pathways: associative and dissociative. In the dissociative pathway, N-O bond activation and breaking occur immediately after the adsorption process, inducing

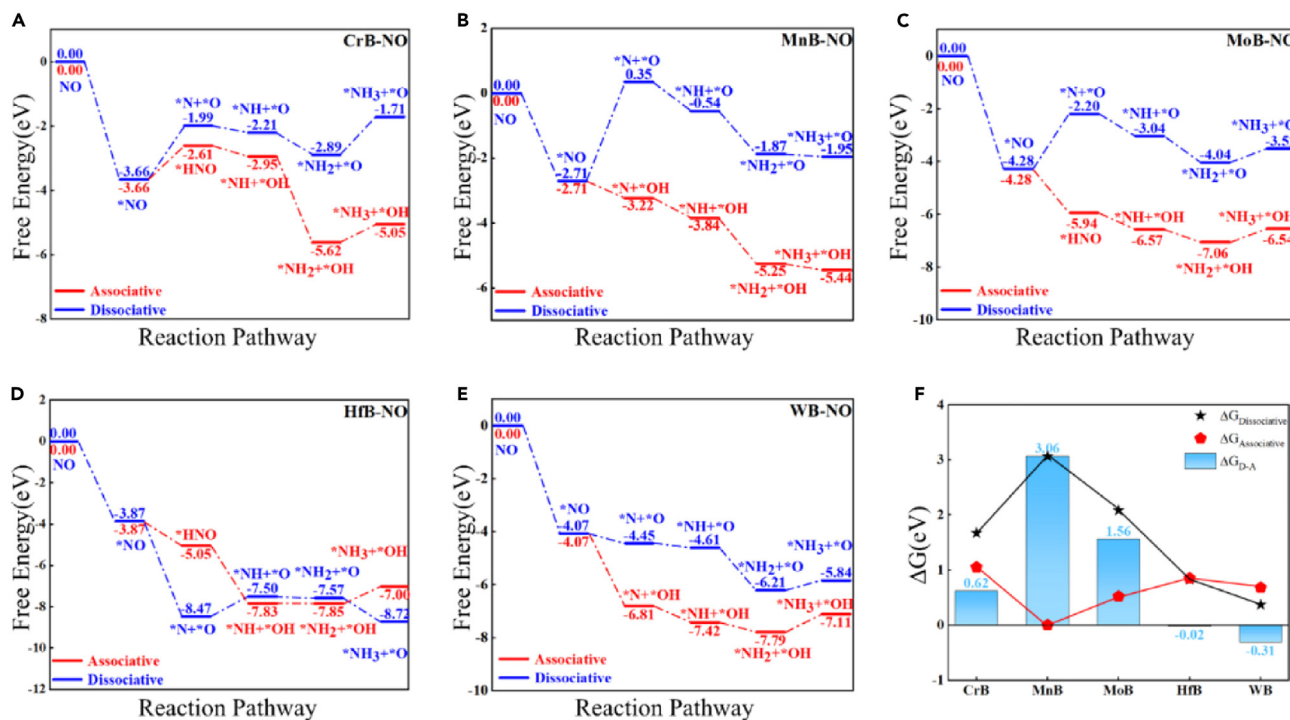


Figure 1. The associative and dissociative mechanisms of NO_xRR

Free-energy diagrams of NH₃ synthesis via associative and dissociative pathways after NO adsorption on (A) CrB, (B) MnB, (C) MoB, (D) HfB, and (E) WB. (F) The energy limit of several substrates in the hydrogenation of NO molecules to NH₃ via dissociative and associative mechanisms. The ΔG_{D-A} in the figure shows the free energy difference of the rate-limiting steps associated with dissociative and associative mechanisms. Reprinted from.⁵⁴ Copyright Elsevier, 2022.

the formation of isolated N and O atoms on the MBenes surface, which will be subsequently converted into NH₃ and H₂O upon the addition of H⁺ + e⁻ as depicted in Figure 1. When producing NH₃ via the associative pathway, the N-O bond is fully activated but not broken when a single NO molecule is adsorbed on the catalyst surface. The subsequent hydrogenation process of the NO molecule involves a selective transfer of hydrogen and electrons into either the N or O atom, producing different reaction intermediates. Hence, it is essential to calculate the adsorption barrier and determine the binding site of the H proton to confirm the intermediates, such as *NOH or *NHO, since the proton binding site in each step will govern the reaction pathways.⁵⁴

CATALYST DESIGNS FOR ELECTROCHEMICAL NO_x REDUCTION REACTION

The design of efficient and durable electrocatalysts for NO_x reduction involves two distinct approaches: computational screening and experimental testing. Computational screening, also known as rational design, involves computer simulations to predict the properties of potential catalysts and select the most promising candidates for experimental validation. This approach is based on the principle that a catalyst's electronic and geometric properties determine its activity and selectivity in a reaction and, by manipulating these properties, one can design more efficient and selective electrocatalysts for NO_x reduction.

Experimental testing, on the other hand, includes synthesizing and testing various electrocatalysts using a range of characterization and performance evaluation techniques to determine their effectiveness in NO_x reduction. This approach can provide critical insights into the real-world performance of catalysts, such as their stability, durability, and ability to operate under varying conditions. Recently, some groups of researchers have focused on high-throughput screening (HTS) techniques to discover the most promising electrocatalysts at unprecedented times. These techniques involve using automated equipment to rapidly test a large number of samples in parallel, allowing for the efficient evaluation of potential catalysts.

Both computational screening and experimental testing play an essential role in developing efficient and durable electrocatalysts for NO_x reduction. For instance, they can design an effective catalyst by searching

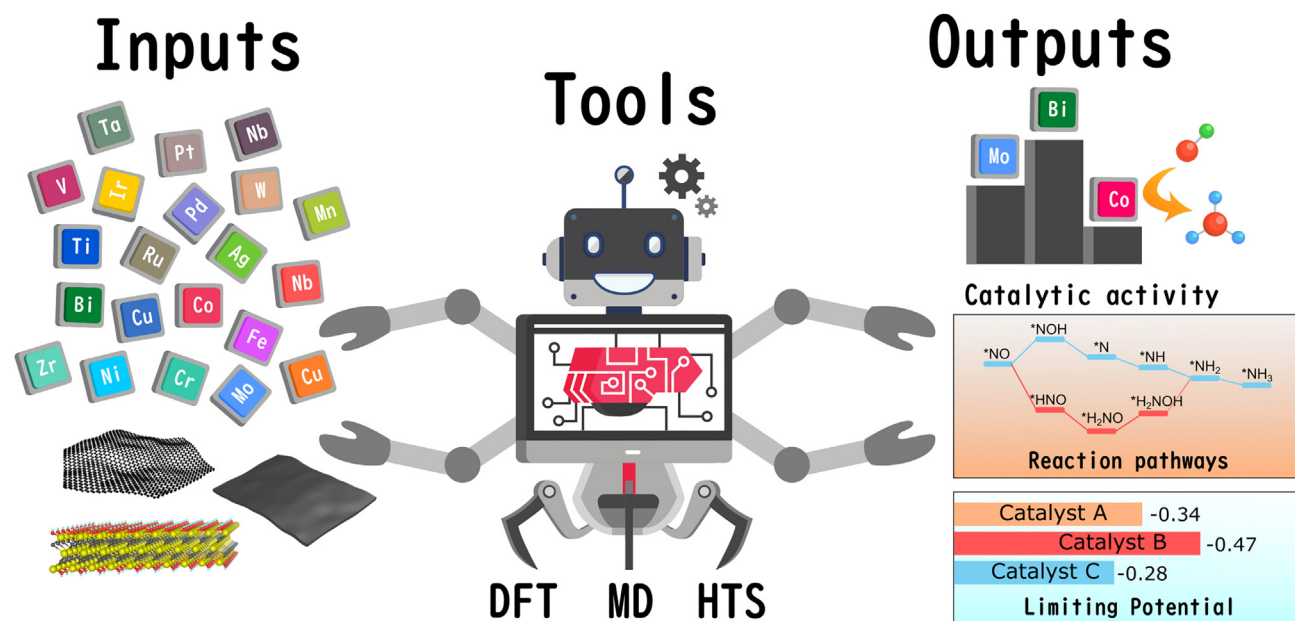


Figure 2. Workflows of NO_x electroreduction catalysts screening via computational simulations

the appropriate active site, the region on the catalyst surface where the reaction occurs. The active site must have the appropriate chemical properties to facilitate the desired reaction, and the size and shape of the active site can also influence the catalyst's performance. In addition to the active site, the overall structure, including the presence of defects or impurities on the catalyst's surface, can also contribute to its performance, such as reaction rate and catalyst yield. By combining these approaches, researchers can design and test a wide range of potential catalysts quickly and cost-effectively, discovering novel and effective electrocatalysts that can help address the urgent problem of NO_x pollution.

COMPUTATIONAL DESIGN OF ELECTROCATALYTIC NO_x REDUCTION CATALYST

Efficient catalyst design is crucial for the practical development of electrochemical NO_x reduction. In the past, countless catalysts were specifically designed with improved performances. Still, computational design has become an important tool for accelerating the discovery of new catalysts, understanding the fundamental mechanisms, and identifying active sites on catalyst surfaces. With the advances in computational abilities, researchers can now design and screen potential catalysts using HTS, reducing the time and cost of traditional trial-and-error experiments.

In the emerging field of NO_xRR, researchers are now mostly screening single- and biatom catalysts along with supporting 2D materials using a range of powerful tools, including DFT, molecular dynamics (MD), and HTS methods, as shown in Figure 2. These simulation tools allow researchers to predict the behavior of materials at the atomic scale and molecular level, and to explore their catalytic properties. The outputs of these simulations include highly optimized catalysts with improved activity and selectivity, identification of limiting potential, exploration of reaction pathways (such as distal or alternating), and active sites on the catalyst surface that facilitate catalytic reactions. This information is invaluable in designing and developing new catalysts as it provides insights into the underlying mechanisms of catalytic reactions, ultimately leading to the development of more efficient and sustainable chemical processes. With the continuous advancement of computational simulation techniques, the possibilities for developing new and highly efficient catalytic materials are limitless.

The primary obstacle in NO_xRR is to fine-tune the product selectivity of the catalysts toward NH₃. To overcome this issue, a methodical screening approach for effective SACs has been suggested utilizing first-principles calculations. SACs have garnered significant attention due to their high metal utilization efficiency and exceptional catalytic activity. Through a study involving 23 transition metals (ranging from Ti to Au) embedded in monolayer N-doped graphene (C₂N), it was discovered that six TM-C₂N could efficiently

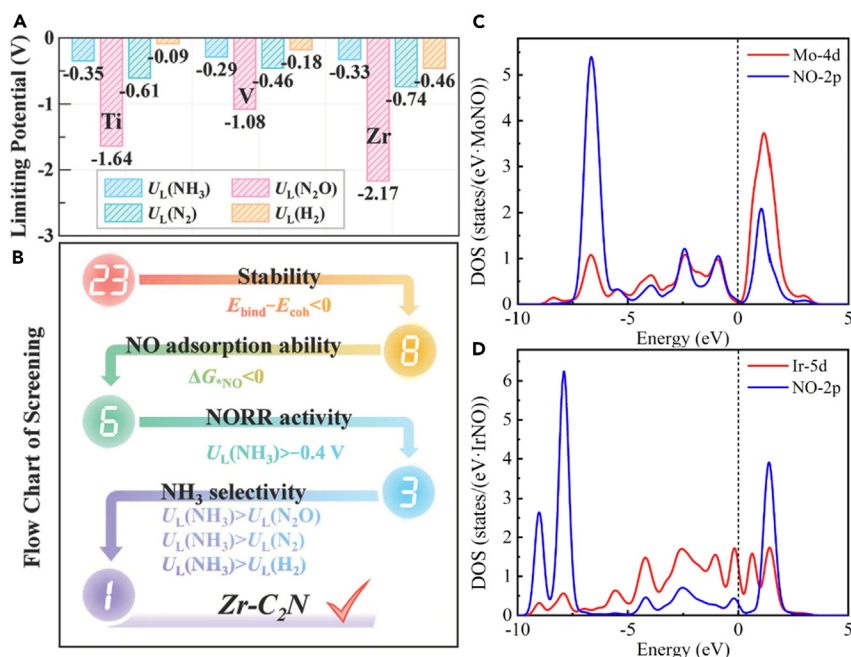


Figure 3. Several promising NO_xRR electrocatalysts

(A) Limiting potentials of Ti-, V-, and Zr-C₂N, (B) Zr-C₂N as promising NO_xRR electrocatalysts, adapted from⁵⁵ with permission, Copyright John Wiley & Sons, Inc. 2021., and (C and D) orbital hybridization between Mo-4d or Ir-5d and N-2p. Reproduced with permission from,⁵⁸ Copyright Elsevier 2022.

adsorb and activate the NO molecule due to the “donation/back donation” mechanism between the TM atom and NO.⁵⁵ When considering the NO_xRR activity toward NH₃, Ti-, V-, and Zr-C₂N display elevated activity levels with less negative limiting potentials of −0.35, −0.29, and −0.33 V, respectively, as shown in Figure 3A. Ultimately, Zr-C₂N is identified as a promising NO_xRR catalyst due to its ability to suppress the formation of byproducts such as N₂O, N₂, and H₂ (Figure 3B). The use of the same supporting materials revealed that V₂/Cr₂/Mn₂/Mo₂-C₂N exhibited the most significant potential in catalyzing NO, with remarkable stability, activity, and selectivity. Moreover, the results showed that the NH₃ synthesis through NO_xRR had a low kinetic barrier when utilizing V₂/Cr₂/Mn₂/Mo₂-C₂N.⁵⁶ Upon analysis, it was found that a substantial charge transfer takes place between NO and TM₂-C₂N, thus providing additional evidence for the “back donation/donation” mechanism of NO adsorption on TM₂-C₂N. The process involves a series of five hydrogenation steps, in which $\text{NO} + 5\text{H}^+ + 5\text{e}^- \rightarrow \text{NH}_3 + \text{H}_2\text{O}$. Moreover, three potential pathways for the direct conversion of NO-to-NH₃ exist: N-end, O-end, and side-on pathways. The adsorption patterns of NO molecules determine which pathway is utilized. As such, this reveals that the method by which NO molecules are adsorbed can greatly impact the conversion efficiency of NO-to-NH₃.

The substitution of supporting materials with B-defected boron phosphide (BP) monolayers led to the discovery of Ti@BP, V@BP, Cu@BP, and Au@BP as the most favorable catalysts.⁵⁷ In the event of nitrogen doping into BP monolayers, Mo- and Ir-anchored N-doped BP were identified as promising electrocatalysts for NO_xRR, showcasing limiting potentials of −0.10 V and −0.06 V, respectively.⁵⁸ These catalysts exhibited significantly greater or at least similar rate constants compared to the exceptional Pt(111) surface. According to electronic analysis, the Mo-4d or Ir-5d orbitals could effectively hybridize with the NO-2p orbitals, providing adequate activation of the adsorbed NO species (Figures 3C and 3D). On the surface of Pt(100), Ti, Cr, Co, and Ni SACs demonstrated remarkable NO_xRR catalytic activity.⁵⁹ Specifically, the Ni-Pt combination displays exceptional activity and selectivity for NO_xRR in NH₃ synthesis. Furthermore, the Ti/Co/Ni-Pt combination exhibits higher selectivity for NO_xRR than the HER. Of the 27 evaluated TM@MoS₂ catalysts (from 3days to 5days period), 19 were found to be both thermodynamically stable and practically feasible in the context of the defective MoS₂ monolayer. Of these catalysts, 13 showed high NO_xRR activity toward NH₃, and six favored the production of NH₂OH. It is noteworthy that the TM@MoS₂ catalysts demonstrated efficacy in suppressing HER and byproducts (N₂O/N₂). Five of the evaluated catalysts (TM = Ni, V, Cr, Nb, Ti) displayed exceptionally low limiting potentials (UL = −0.18 to 0 V) in producing

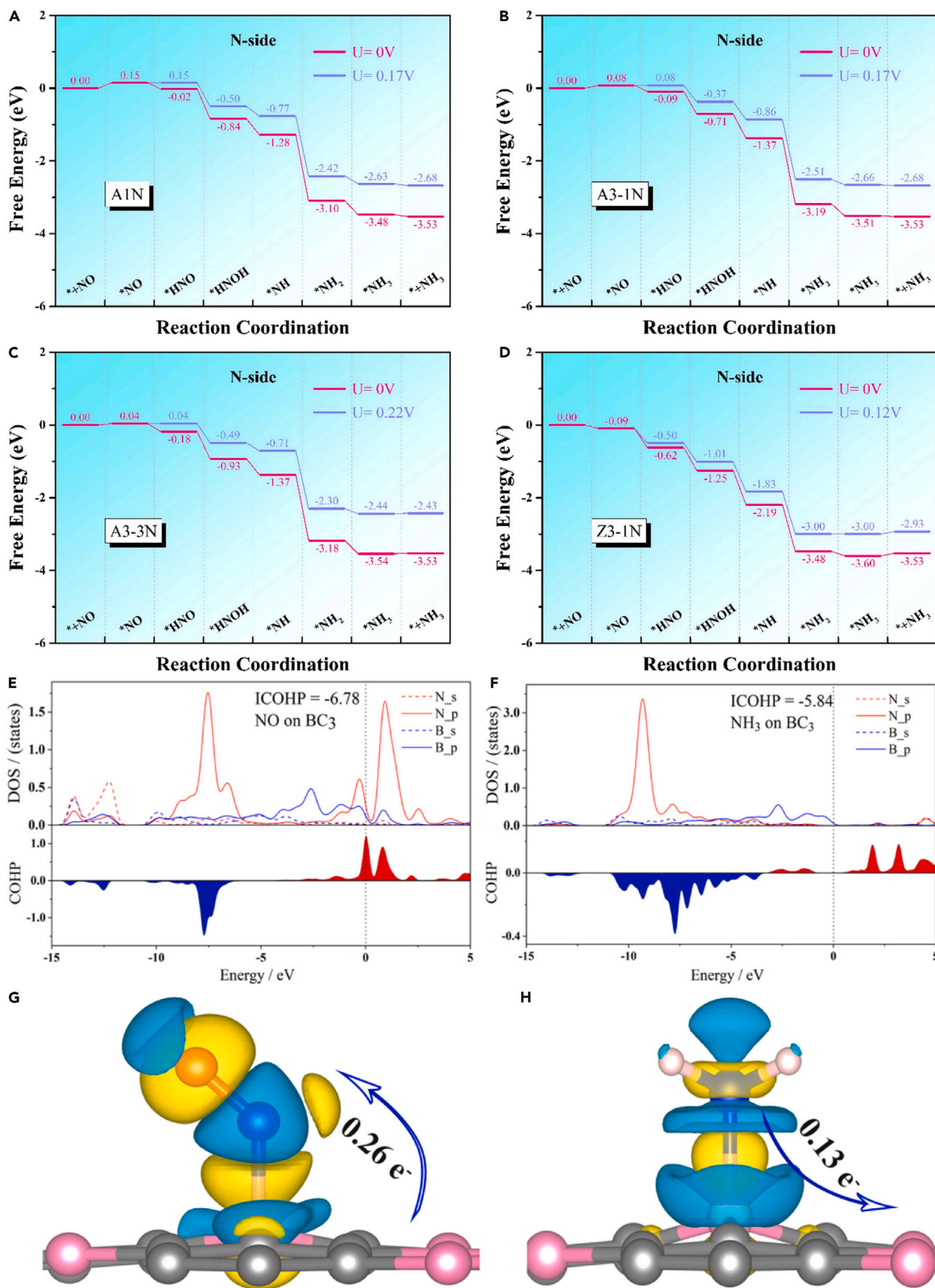


Figure 4. NO_xRR activity of using NO on hBN-graphene and BC₃

(A–D) Gibbs free energy diagrams representing the NO_xRR of four structures (A1N, A3-1N, A3-3N, and Z3-1N) are displayed using gaseous NO as the reference potential, with the preferred pathway illustrated under zero (pink) and limiting potential (blue) conditions. (E and F) Representation of the PDOS of NO and NH₃ adsorbed on the BC₃ surface, along with ICOHP analysis of the relevant regions. The bonded states are highlighted in blue, while the anti-bonded states are represented in red. (G and H) Graphical depictions of the charge difference density, with areas of electron accumulation in yellow and electron loss in blue. The iso-surface value is 0.005 e⁻/Bohr.³ Reproduced with permission from⁶³ and⁶⁴ Copyright Elsevier 2022.

NH₃, while two (TM = Ag and Pt) generated NH₂OH with a UL of 0 V.⁶⁰ Co- and Rh-HAB (hexaaminobenzene) MOFs were investigated as potential electrocatalysts for NO_xRR by Huang et al.⁶¹ Computational simulations showed that both MOFs had moderate NO adsorption strength to the substrate, making them promising candidates for NO_xRR catalytic activity. Furthermore, the calculations demonstrated that the Co-HAB MOF was the most effective electrocatalyst for NO_xRR, capable of generating NH₃ at a low NO coverage with a limiting potential of -0.26 V.

The design of bilayer single-atom catalysts (BSACs) with adjustable surface chemistry has been suggested as a universal approach to heterogeneous catalysis.⁶² Heterogeneous BSACs have exhibited a propensity for augmenting the capture and activation of NO_x, which is critical for electrochemical NH₃ synthesis. The inversion symmetry breaking inherent in these BSACs engenders a built-in electric field around the active sites that can be tuned to optimize the catalytic performance for NO_xRR, including encompassing NO_x adsorption and activation, limiting potential, selectivity, and reaction pathway. After subjecting a range of homonuclear M₂-CmNn-GN BSACs and their heterogeneous counterparts to high-throughput calculations, three systems, specifically TiV-N₄, NbV-N₄, and GaV-N₄-GN, were determined to be effective in suppressing competitive HER while exhibiting limiting potentials of -0.32, -0.20, and -0.25 V, respectively.

2D materials can serve as a supporting platform and a standalone electrocatalyst for activating and hydrogenating NO_x molecules. To this end, researchers proposed a metal-free NO_xRR catalyst design using hexagonal boron nitride-graphene (hBN-graphene) heterostructures with a C_{center}-CN₂ configuration.⁶³ The modified hBN-graphene interface resulted in impressive NO_xRR activity, achieving a low limiting potential of -0.22 V. In addition, the hBN-graphene heterostructures effectively inhibited HER and showed considerable thermal stability according to ab-initio MD simulations. By assessing the catalytic activity of NO_xRR through two general reaction pathways, the N-side pathway emerges as the preferred route over the O-side pathway. In the O-side pathway, the rate-determining steps involve the formation of H₂O and the first hydrogenation of NO, while the initial hydrogenation of NO and subsequent hydrogenation steps are the pivotal steps in the N-side pathway. The first hydrogenation step demonstrates a better thermodynamic preference for the N atom, underscoring the N-side pathway's preference for NO_xRR on the modified hBN-graphene heterostructures. The armchair structures exhibit exceptional NO_xRR catalytic activity, reaching a sufficiently low limiting potential of about -0.2 V. However, despite the low energy barrier of the first hydrogenation step in structure Z3-1N, it cannot catalyze the step *NH₂ → *NH₃ efficiently.⁶³ Figures 4A–4D displays the overall NO_xRR of hBN-graphene.

Recently, a study highlighted the exceptional catalytic activity of BC₃ 2D materials, producing an astonishingly low limiting potential of -0.29/-0.11 V.⁶⁴ The three reaction pathways, including NO_(g) + 5H⁺ + 5e⁻ → NH₃ (g) + H₂O, were observed, and the mechanism behind NO activation and NH₃ adsorption/desorption was explained by examining the density of states and ICOHP of adsorbed NO and NH₃ on the BC₃ surface. Figure 4E illustrates that the NO intermediate gets attached to the B site, where the p orbital electrons of N and B atoms have significant involvement. The opposing bonding state suggests that the N-B bond formation is hindered due to the strong interaction between N and B. The electron cloud of the B atom interacts with NO, leading to the formation of the N-B bond. Figure 4G demonstrates an increment in the electron density, leading to better interaction between NO and BC₃. A single N atom active site is produced when the proton-electron pairs attack the O atom in NO. Figure 4F reveals that the s and p orbitals of the B atom interact with the p orbital of the N atom, responsible for the adsorption of NH₃ on the BC₃ surface. Figure 4H depicts a reduction in the electron density of the N atom, while an increase in the electron density is observed in the area around the B atom. By conducting a Bader charge analysis, it was discovered that the BC₃ surface undergoes an electron transfer of 0.13 e⁻.⁶⁴

Another 2D material, so-called MXenes, also showed a promising NO_xRR electrocatalytic activity with a limiting potential of -1.09 V (bare Ti₂C) to -0.08 V (Ti₂CS₂) and -0.14 V (Ti₂CO₂).⁶⁵ Although no

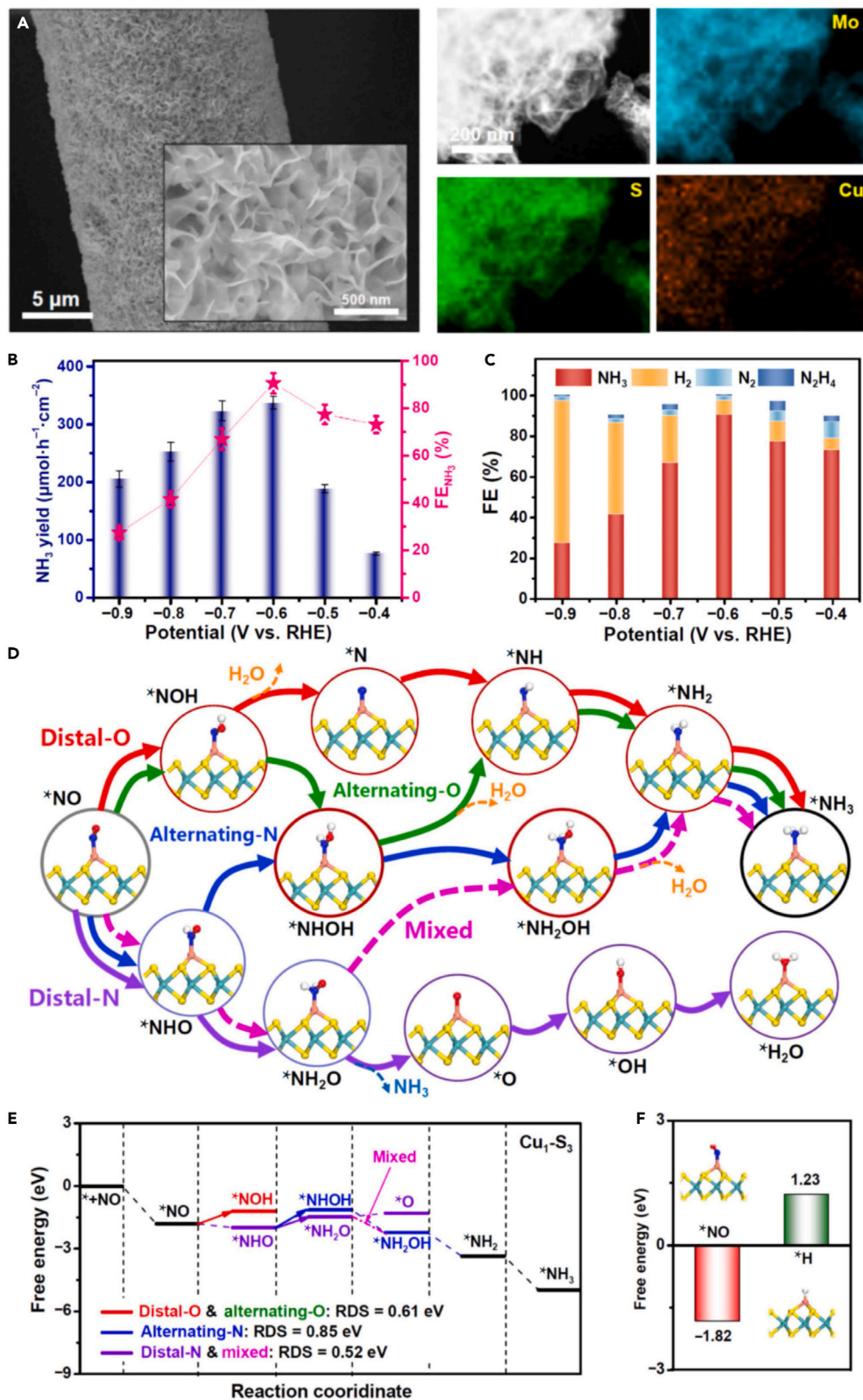


Figure 5. Single-atomic Cu anchored on MoS₂ nanosheets

- (A) SEM images and the corresponding EDS mapping of Cu/MoS₂.
- (B) NH₃ yields and FE of Cu₁/MoS₂ at various potentials.
- (C) FEs of different products after bulk electrolysis for an hour.
- (D) Schematic of different NO_xRR pathways.
- (E) Free energy diagrams of NO_xRR pathways on Cu₁/MoS₂.
- (F) Binding free energies of *NO and *H on Cu₁-S₃. Adapted from⁷², Copyright Springer Nature 2022.

experimental effort has been attempted for these emerging 2D materials, MXenes have shown electrochemical reduction activity and stability for CO₂RR.⁶⁶ In conclusion, the advancements in computational simulation and theoretical calculations have led to the discovery of a wide range of promising electrocatalysts. These findings shed light on the underlying mechanisms of catalysis and offer a practical and efficient means of designing new and improved materials for energy conversion and storage applications.

Catalyst design by experimentation

The performance of electrocatalysts to convert NO_x molecules into NH₃ strongly depends on their composition and structure. While the intrinsic composition of electrocatalysts will determine the adsorption behavior of NO_x molecules and thus affect reaction pathways, the structures of catalysts are intended to boost efficiency and product selectivity. In this section, we discuss recent advances in the development of electrocatalysts for NO_x electrochemical reduction, emphasizing catalyst compositions and various engineering strategies.

Single-atom catalysts (SACs)

SACs are an emerging group of catalysts composed of individual metal atoms attached to a supporting material. Due to their near-complete atomic utilization and excellent catalytic performance, SACs have become increasingly popular.^{67,68} In 2011, Zhang et al. conducted the first research on SACs, where single Pt atoms were synthesized and anchored on iron oxide. They observed that SACs exhibited exceptional stability and catalytic activity, particularly in the oxidation of CO.⁶⁹ Since then, a series of SACs have been reported, which include noble and non-noble metals. SACs have additional advantages over conventional nanoparticle-based catalysts due to their sizes, structural effects, and strong metal-support interactions. The coordination environment of the metal atoms in SACs also plays a critical role in determining their catalytic properties.⁷⁰ Recent research has focused on the promising applications of SACs in the NO_xRR.

Researchers have synthesized a group of electrocatalysts by combining individual metal atoms (Al, Mn, Fe, Cu, and Nb) with B,N co-doped carbon nanotubes.⁷¹ These catalysts have shown remarkable efficiency for ambient electrosynthesis of NH₃, with the single-atomic-site Nb catalyst generating an NH₃ yield rate of $8.2 \times 10^{-8} \text{ mol cm}^{-2} \text{ s}^{-1}$. This exceeds the efficiency of the best-known NRR catalysts by a hundred times and nearly meets the US Department of Energy (DOE) target. The superior performance of the Nb catalyst has been attributed to the presence of single Nb-B₂N₂ sites in it. Theoretical computations have suggested that these sites enable NO adsorption and reduce the energy barrier of the potential-determining step. A remarkable record in electrochemical NH₃ synthesis rate was established using commercially available Cu electrodes, with $517.1 \mu\text{mol h}^{-1} \text{ cm}^{-2}$ achieved at -0.9 V vs. RHE , accompanied by an FE (Faradaic efficiency) of 93.5%.²⁶ Furthermore, single-atomic Cu anchored on MoS₂ nanosheets (SEM and EDS mapping) is shown in Figure 5A. At -0.6 V vs. RHE , this catalyst exhibited outstanding performance, achieving an NH₃ yield rate of $337.5 \mu\text{mol h}^{-1} \text{ cm}^{-2}$ and an FE of 90.6%, surpassing nearly all previously reported NO_xRR catalysts. (Figures 5B and 5C).⁷² By utilizing a combination of DFT, MD simulations, and ab initio MD (AIMD) simulations, it was discovered that the activation and hydrogenation of NO were achieved through a mixed pathway (distal and alternating) with Cu-anchored MoS₂ catalysts. This simultaneous retardation of proton coverage led to high activity and selectivity for the NO_xRR at the atomic level. (Figures 5D–5F). The NO_xRR process has been successfully achieved using Cu/porous-TiO₂ binary catalysts.⁷³ The utilization of porous TiO₂ with ultrafine Cu nanoparticles on its surface can provide greater surface areas and channels for superior NO adsorption capacity while suppressing the agglomeration of Cu nanoparticles. The electrocatalytic performance of the Cu/P-TiO₂ electrode was remarkable, resulting in an NH₃ yield of $207.1 \mu\text{mol h}^{-1} \text{ mg}^{-1}$ and an FE of 86.5% at -0.3 V vs. RHE in 0.1 M K₂SO₄.⁷³

Other promising SACs are bismuth (Bi) and gold (Au).⁷⁴ Bi possessed high adsorption energy for hydrogen; thus, the competing HER can be suppressed. However, its inferior electrical conductivity due to its

semiconductor nature limits its electrocatalytic activity. To overcome this limitation, Bi nanoparticles anchored in carbon nanosheet (Bi@C) have been developed, exhibiting an impressive NH_3 yield of $93.7 \mu\text{mol h}^{-1} \text{mg}_{\text{cat.}}^{-1}$ and a high FE of 93.0% in 0.1 M Na_2SO_4 electrolyte.⁷⁵ At a potential of -0.65 V , Bi powder yielded NH_3 via NO reduction at a rate of $6 \pm 2 \times 10^2 \text{ pmol s}^{-1} \text{cm}^{-2}$, while the use of Au/C resulted in an NH_3 production rate of $8.1 \pm 0.9 \times 10^2 \text{ pmol s}^{-1} \text{cm}^{-2}$ at -0.30 V .⁷⁴ Co SACs are highly active and durable in NO_xRR when anchored on MoS_2 (Co/MoS₂).⁷⁶ Co/MoS₂ exhibited excellent NO_xRR performances, selectively absorbed NO molecules, and promoted the hydrogenation energetics of the NO_xRR process, leading to a high NH_3 yield of $217.6 \mu\text{mol h}^{-1} \text{cm}^{-2}$ and an NH_3 -FE of 87.7% at -0.5 V vs. RHE. Recent studies suggested that W single atoms could efficiently activate nitrogenous molecules, indicating the potential of W-SACs in NO_xRR . A single-atom W confined in MoO_{3-x} amorphous nanosheets (W/MoO_{3-x}) was designed. W/MoO_{3-x} had the highest FE of 91.2% and NH_3 yield rate of $308.6 \mu\text{mol h}^{-1} \text{cm}^{-2}$.⁷⁷ Using other catalysts, such as p-block Sb,⁷⁸ Ir,⁷⁹ and In⁸⁰ anchored in amorphous a-MoO₃ yield an NH_3 rate of $273.5 \mu\text{mol h}^{-1} \text{cm}^{-2}$, $438.8 \mu\text{mol h}^{-1} \text{cm}^{-2}$, and $242.6 \mu\text{mol h}^{-1} \text{cm}^{-2}$ at -0.6 V vs. RHE, respectively. The isolated Sb and Ir atoms in O vacancies of amorphous MoO₃ powerfully activated and hydrogenated NO with a near-zero energy barrier. The isolated Sb atoms anchored in Sb₂S₃ have also shown selective NO_xRR with high yield and FE.⁸¹

In conclusion, SACs have shown great promise for diverse electrolytic reactions due to their unique properties of high atomic utilization and low-coordination environment. SACs should be anchored on supported materials to prevent the aggregation process. Amorphous substrates with abundant vacancies and dangling bonds can provide confined spaces to anchor metal atoms and induce a strong metal-substrate interaction, making them an attractive platform for SACs. Table 1 shows the recent progress of SACs for electrocatalytic NO_xRR .

Transition metal dichalcogenides

Nanostructures based on transition metal dichalcogenides (TMDs) have recently emerged as appealing electrocatalysts for various electrocatalytic reactions, including NO_xRR , owing to their excellent properties. Despite their surface-active site on their 2D structures,⁸² TMDs have barely been investigated as efficient noble metals and SACs compared to other materials. A detailed discussion on the synthesis and properties of TMDs can be found elsewhere.⁸³ To clarify their catalytic activity and product selectivity, a thorough evaluation of some representative 1T' phase single layer TMDs such as MoS₂, MoSe₂, MoTe₂, TaTe₂, and WTe₂ was conducted using first-principle calculations.⁸⁴ Investigating the reaction pathway is critical to designing the most efficient TMDs catalysts. In 1T'-TMDs, NO molecules are adsorbed at a sulfur vacancy site and favorably undergo two hydrogenation pathways, leading to the formation of NH_3 . A possible reaction pathway under low coverage is consistent with the reaction $*\text{NO} \rightarrow *\text{NOH} \rightarrow *\text{N} \rightarrow *\text{NH} \rightarrow *\text{NH}_2 \rightarrow *\text{NH}_3$. Under high NO coverage, 1T'-TMDs yield N_2O or N_2 via different pathways.⁸⁴ To suppress the competing HER, surface-defected 1T'-MoS₂, 1T'-MoSe₂, 1T'-MoTe₂, 1T'-WTe₂, and 1T'-TaTe₂ catalysts with S and Se vacancies are introduced, as the Gibbs free adsorption energies of H are much weaker than those of $*\text{NO}$ in a defected surface.⁸⁴ The high catalytic activity of these catalysts for NO_xRR arises from a large amount of activated NO at the $*\text{NO}$, where the electron is accumulated on $*\text{NO}$, and the depleted regions are in adjacent metals.

Experimental results support the excellent performance of TMDs toward highly selective electrochemical NO reduction. For instance, MoS₂ nanosheets were grown on graphite felt (GF) to construct 3D MoS₂/GF nanoarchitectures. Under acidic conditions (0.1 M HCl), MoS₂/GF achieves an FE of 76.6% and up to $99.6 \mu\text{mol cm}^{-2} \text{h}^{-1}$ of NH_3 yield. The NH_3 yield remained almost unchanged after repeated cycles, indicating the excellent electrochemical long-term stability of MoS₂/GF (Figures 6A and 6B). The DFT calculation has provided an intuitive insight into the catalytic mechanism. According to the calculation, NO molecules tend to adsorb side-on at the Mo-Mo bridge (B) site, which has a stronger bond strength than H on the positively charged metal sites, thus suggesting the potential suppression of competing HER. The surface-terminated Mo atoms may also effectively catalyze and activate NO_x molecules, as seen in the Mo₂C case.⁸⁵ Figures 6C and 6D shows the NO_xRR pathway to NH_3 involving Mo₂C/GF. Furthermore, the MoS₂/GF can be used as a cathode in a Zn-NO battery device, delivering a power density of 1.04 mW cm^{-2} with $24.2 \mu\text{mol h}^{-1} \text{mg}_{\text{cat.}}^{-1}$ NH_3 yield. This presents an opportunity to tackle NO pollutants more sustainably by removing NO while generating electricity and chemical feedstocks. Table 1 shows the recent progress of TMDs for electrocatalytic NO_xRR .

Carbon-based electrocatalysts

The creation of catalysts devoid of noble metals that can drive the NO_xRR reaction would open up the possibility for broader-scale utilization of NH_3 synthesis via electrochemical NO reduction. Carbon-based

Table 1. Electrocatalytic NO_xRR performance of SACs, TMDs, carbon-based, and metal alloys electrocatalysts

Catalysts	Electrolyte, membrane, cell	NH ₃ yield	FE (%), potential vs. RHE	By product	Reference
Binanodendrites	0.1 M Na ₂ SO ₄ , H-type cell, Nafion 117	70.2 μmol h ⁻¹ mg _{cat.} ⁻¹	89.2% at -0.5 V	N ₂ , N ₂ H ₄ , H ₂	Lin, et al. ⁹²
Cu	0.1 M NaOH +0.9 M NaClO ₄ , gas-fed three-compartment flow cell, Nafion 117	-	83.5% at 0.08 V	N ₂ , N ₂ O, NH ₂ OH	Ko, et al. ⁹³
Co			44.7% at -0.03 V		
Pt			22.2% at 0.04 V		
Cu foam	0.25 M Li ₂ SO ₄ , H-type cell, Nafion 115	517.1 μmol h ⁻¹ cm ⁻²	93.5% at -0.9 V	N ₂ , N ₂ O, H ₂	Long, et al. ²⁶
Ir	0.5 M Na ₂ SO ₄ , H-type cell, Nafion 117	438.8 μmol h ⁻¹ cm ⁻²	92.3% at -0.47 V	H ₂ , N ₂ H ₄ , N ₂ O	Chen, et al. ⁷⁹
Co	0.5 M Na ₂ SO ₄ , H-type cell, Nafion 117	217.6 μmol h ⁻¹ cm ⁻²	87.7% at -0.5 V	H ₂ , N ₂ H ₄ , N ₂	Li, et al. ⁷⁶
BiNPs@carbon NS	0.1 M Na ₂ SO ₄ + 0.05 mM Fe(II)EDTA, H-type cell, Nafion 117	93.7 μmol h ⁻¹ mg _{cat.} ⁻¹	93.0% at -0.4 V	H ₂	Liu, et al. ⁷⁵
Ru nanosheets	0.5 M Na ₂ SO ₄ , H-type cell, Nafion 117	45.0 μmol h ⁻¹ mg _{cat.} ⁻¹	66.0% at -0.2 V	H ₂	Li, et al. ⁹⁴
MoS ₂ nanosheet on graphite felt (MoS ₂ /GF)	0.1 M HCl, H-type cell, Nafion 117	99.6 μmol cm ⁻² h ⁻¹	76.6% at -0.7 V	N ₂ H ₄	, et al. ³⁴
Cu/MoS ₂	0.5 M Na ₂ SO ₄ , H-type cell, Nafion 117	337.5 μmol h ⁻¹ cm ⁻²	90.6% at -0.6 V	-	Chen, et al. ⁷²
P-doped MoS ₂	0.1 M [C4mpyr][eFAP], H-type cell, Nafion 211	22.8 μmol h ⁻¹ mg _{cat.} ⁻¹	69.0% at -0.6 V	-	Wei, et al. ⁹⁵
Fe-doped MoS _{2-x}	0.5 M Na ₂ SO ₄ , H-type cell, Nafion 117	288.2 μmol h ⁻¹ cm ⁻²	82.5% at -0.6 V	H ₂ , N ₂ H ₄ , N ₂	Chen, et al. ⁹⁶
Honeycomb carbon nanofiber (CNFs)	0.2 M Na ₂ SO ₄ , H-type cell, Nafion 117	22.4 μmol h ⁻¹ cm ⁻²	88.8% at -0.6 V	N ₂ H ₄ , H ₂	Ouyang, et al. ⁸⁶
Au/rGO	0.5 M Na ₂ SO ₄ , three-electrodes cell	14.6 μmol h ⁻¹ cm ⁻²	65.2% at -0.1 V	H ₂	Xiong, et al. ²⁵
Epoxy-functionalized carbon	0.1 M PBS +0.2 M Na ₂ SO ₃ , H-type cell, Nafion 117	-	83.3% at -1.1 V vs. SCE	N ₂ , N ₂ O	Sharif, et al. ⁸⁸
Nb-supported B, N co-doped CNT	0.1 M HCl, three-channel flow cell, Nafion 117	2952.0 μmol h ⁻¹ cm ⁻²	77.0% at -0.6 V	-	Peng, et al. ⁷¹
g-C ₃ N ₄ nanosheets	0.1 M PBS, H-type cell, Nafion 117	30.7 μmol h ⁻¹ cm ⁻²	45.6% at -0.4 V	H ₂	Li, et al. ⁹⁷
Cu-Ti hollow fibers	0.05 M H ₂ SO ₄ , H-type cell, Nafion 117	400.0 μmol cm ⁻² h ⁻¹	90.0% at -0.6 V	H ₂ , N ₂ O, N ₂	Shi, et al. ⁸⁹
CuFe	0.1 M PBS, H-type cell, Nafion 117	100 μmol h ⁻¹ cm ⁻²	90.6% at -0.8 V	-	Hao, et al. ²⁹
PdCu	0.5 M NaOH, three-electrode cell	-	24.1% at -0.9 V	N ₂ H ₄ , N ₂ , H ₂	Soto-Hernández, et al. ²⁴
Cu _{1-x} Ru _x	0.5 M Na ₂ SO ₄ , H-type cell, Nafion 117	17.7 μmol h ⁻¹ cm ⁻²	64.9% at -1.1 V	-	Soto-Hernández, et al. ²⁴
RuGa	0.1 M K ₂ SO ₄ , H-type cell, Nafion 117	320.6 μmol h ⁻¹ mg _{cat.} ⁻¹	72.3% at -0.2 V	-	Zhang, et al. ⁹¹

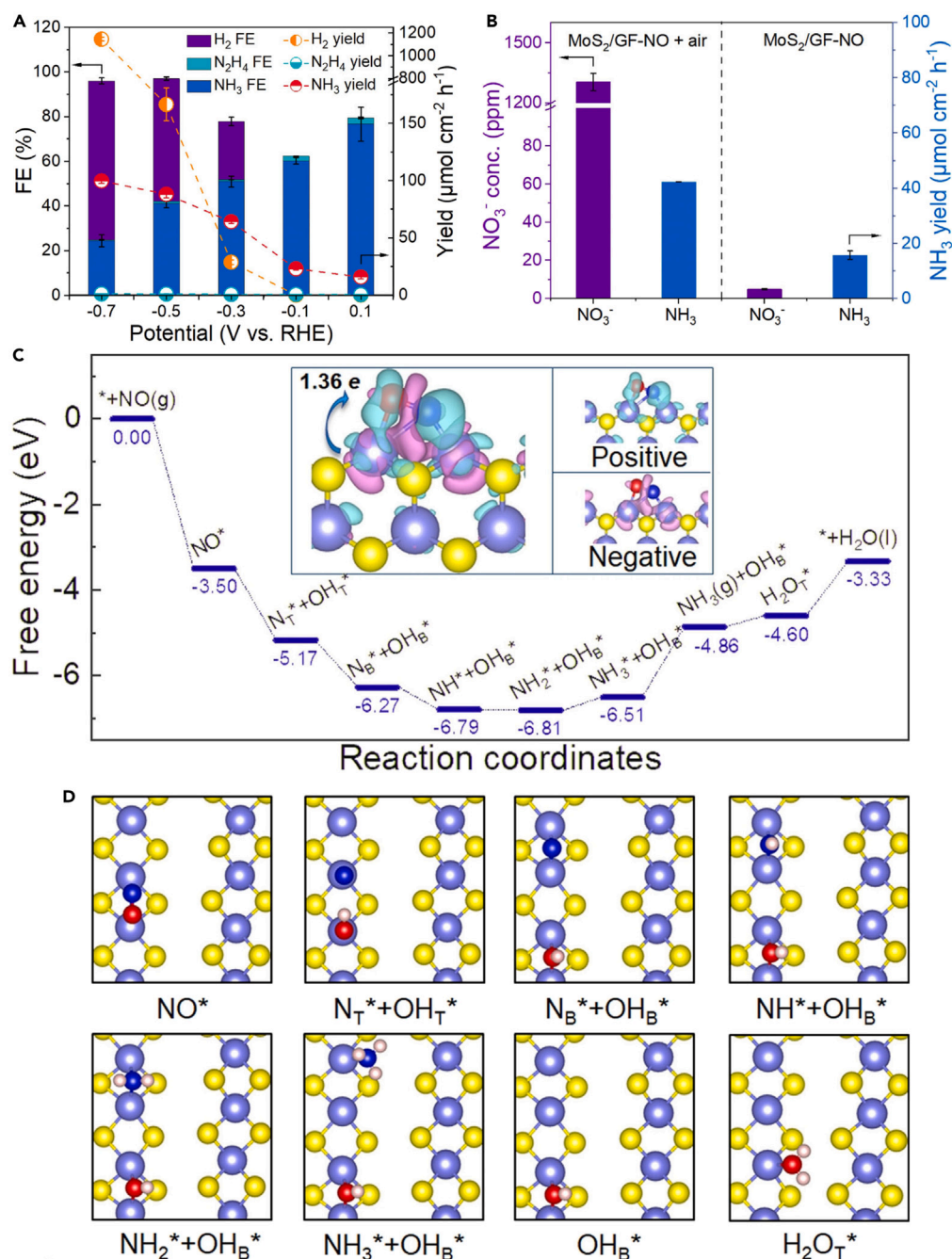


Figure 6. MoS₂ nanosheets on graphite felt (GF) to construct 3D MoS₂/GF nanoarchitectures

(A) The distribution of products for MoS₂/GF at different potentials.

(B) The NH₃ yield and the concentration of NO₃⁻ for MoS₂/GF after 1 h of electrolysis in gas-tight and open chambers.

(C and D) The free energy landscape for NO_xRR on MoS₂(101) and corresponding atomic structures of the intermediates. The local density of states (DOS) of the adsorbed NO and its bonded Mo atoms is also shown. The insets in (C) represent charge density differences for the adsorbed NO, where cyan and red regions indicate electron accumulation and loss, respectively. The topmost atomic layer of the substrate and the adsorbed intermediates are shown in (D) for clarity, with Mo represented by light blue spheres, S by yellow spheres, N by dark blue spheres, O by red spheres, and H by pink spheres. Reproduced with permission from: ³⁴ Copyright WILEY-VCH Verlag GmbH & Co. KGaA, Weinheim 2021.

materials have proven to be highly effective electrocatalysts and supported in a wide range of electrocatalytic applications, including N_2 reduction (NRR), O_2 reduction (ORR), and CO_2 reduction (CO_2RR), owing to their exceptional electrical conductivity, electrochemical stability, and corrosion resistance. Among the many advantages of carbon-based catalysts is the abundance of carbon, which is readily available in various forms of hydrocarbon compounds from biomass waste. This makes producing carbon-based catalysts from biomass an attractive and sustainable approach. Additionally, due to the diverse range of carbon allotropes, carbon-based catalysts can be systematically designed into various shapes, including 0D (carbon nano- or quantum dots), 1D (carbon nanofibers), 2D (rGO, GO), and 3D monoliths.

Carbon nanofibers, through peroxidation and carbonization processes, can be transformed from a smooth surface into a structure resembling a honeycomb with interconnected and open nanocavities.⁸⁶ As a result, the specific surface area of the carbon nanofiber catalyst is increased, allowing for a high NH_3 yield of $22.4 \mu\text{mol h}^{-1} \text{cm}^{-2}$ with an FE of up to 88.3%. DFT calculations suggest that the most active centers for NO adsorption and activation are $-\text{OH}$ groups.

In the 2D form, rGO/Au nanocomposites could yield NH_3 of $14.6 \mu\text{mol h}^{-1} \text{cm}^{-2}$ with an FE of 65.2% at neutral pH, which was further increased to 98.3% at acidic conditions (pH = 1).²⁵ Moreover, 2D boron carbide ($\text{B}_{2.6}\text{C}$) grown on a Ti/TiO₂ electrode showed remarkable NO_xRR activity coupled with long-term durability toward NH_3 synthesis and Zn-NO battery.⁸⁷ It produced a yield of $216.4 \mu\text{mol h}^{-1} \text{cm}^{-2}$ and an FE of 87.6% as nanocatalysts for NO electroreduction, and a power density of 1.7mW cm^{-2} with an NH_3 yield of $66.2 \mu\text{mol h}^{-1} \text{cm}^{-2}$ as Zn-NO battery device. DFT calculations have shown that the bonding between B and C atoms transfers electrons to NO orbitals, thus allowing NO to be activated and reduced with less energy requirement (1.48 eV).

Finally, 3D monolithic carbon with abundant hierarchical nano- and mesopore structures obtained from carbonization and CO_2 -activation of biomass have demonstrated excellent efficiency toward electrochemical NO_x reduction, achieving an $\sim 83.3\%$ FE under ambient conditions (neutral pH and room temperature) as well as excellent stability up to 168 h.⁸⁸ The recent progress of electrocatalytic NO_xRR performance of carbon-based electrocatalysts is shown in Table 1.

Metal alloys

As previously discussed, recent studies have shown promising results in the electrochemical reduction of NO using SACs consisting of mono-metallic elements such as Ir, Pt, Rh, Ru, Pd, Cu, Ni, Ag, and Au. However, achieving low-cost production while maintaining (or even enhancing) the catalytic activity of metal nanocatalysts remains challenging. Cu is a benchmark NO_xRR catalyst due to its low-cost fabrication, but it suffers from low selectivity. One strategy to improve its selectivity is to alloy Cu with other metallic elements. Cu has been alloyed with Ti,⁸⁹ Fe,²⁹ Pd,²⁴ Ru,⁹⁰ and Ga,⁹¹ all of which have significantly enhanced the conversion of NO_x molecules to NH_3 . For example, adding Pd atoms to Cu to fabricate PdCu nanoalloy catalysts significantly suppressed the competing HER, facilitating the transfer of protons to NO_x molecules to drive the NO_xRR .²⁴ PdCu catalysts exhibited six times higher catalytic activity than pristine Cu or Pd. Similarly, adding a small amount of Ru to Cu nanoparticles could improve electrocatalytic performance for NH_3 synthesis (FE: 64.9%, NH_3 yield: $17.7 \mu\text{mol h}^{-1} \text{cm}_{\text{cat}}^{-2}$), surpassing that of pristine Cu (FE: 33.0%, NH_3 yield: $5.73 \mu\text{mol h}^{-1} \text{cm}_{\text{cat}}^{-2}$).⁹⁰ The $\text{Ru}_x\text{Cu}_{1-x}$ nanoalloy was fabricated using an *in situ* electrochemical reduction conversion approach. Using differential electrochemical mass spectrometry (DEMS), it was discovered that the electronic transfer from Ru to Cu resulted in a downshift of Cu d-band center, facilitating the rate-limiting hydrogenation step and reducing NH_3 desorption energy, which should lead to high NH_3 yield ($17.7 \mu\text{mol h}^{-1} \text{cm}^{-2}$) and FE (64.9% at -1.1V) as depicted in Figure 7.⁹⁰ Furthermore, when Cu was alloyed with Fe, the resulting CuFe nanoalloy showed promise as a highly effective and versatile catalyst for the NO_x -based pollutants (NO , NO_2 , NO_2^- , and NO_3^-) electroreduction to NH_3 .²⁹ The presence of Cu and Fe atoms in the nanoalloy led to a synergistic effect that lowered the free energy and promoted the hydrogenation process, as revealed by experimental and theoretical investigations. The low-cost CuFe catalyst alloy can treat water and atmosphere pollutants and convert them into valuable chemicals.

Despite exhibiting remarkable NO_xRR activity, developing metal alloy electrocatalysts for electrochemical NO_x reduction necessitates meticulous consideration of various challenges and a concerted effort to overcome them. This is because, compared to noble metal catalysts such as Pt, the electrocatalytic activity of

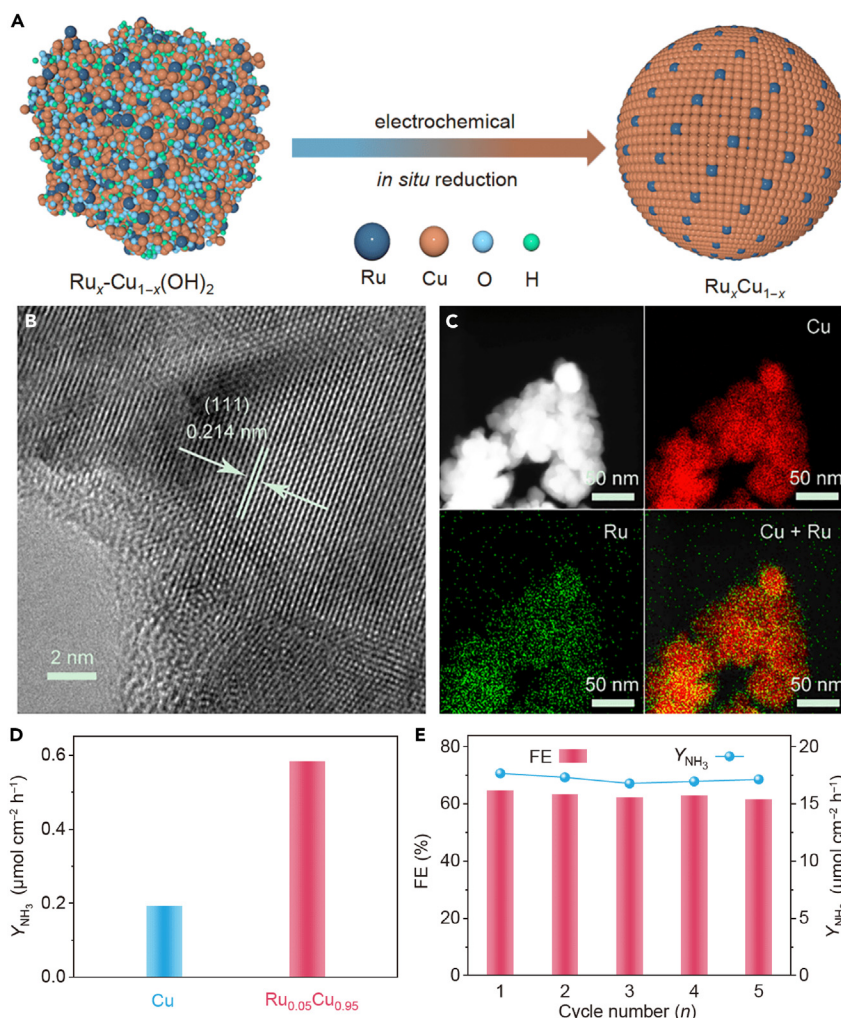


Figure 7. The $\text{Ru}_x\text{Cu}_{1-x}$ nanoalloy using an in situ electrochemical reduction conversion approach

(A) A graphical scheme for synthesizing $\text{Ru}_x\text{Cu}_{1-x}$.

(B) HRTEM image of $\text{Ru}_{0.05}\text{Cu}_{0.95}$.

(C) HAADF-STEM image and the corresponding EDX mapping images of $\text{Ru}_{0.05}\text{Cu}_{0.95}$.

(D) NH_3 rate over Cu and $\text{Ru}_{0.05}\text{Cu}_{0.95}$ after ECSA normalization.

(E) The FE of NH_3 production and corresponding yield rate measured during the recycling tests of NO_xRR over $\text{Ru}_{0.05}\text{Cu}_{0.95}$ at a potential of -1.1 V vs. Ag/AgCl. Reprinted with permission from⁹⁰, Copyright Springer Nature, Inc. 2021.

metal alloy electrocatalysts for NO_x reduction is typically lower. Consequently, higher overpotentials are required to attain the desired reduction reaction, which can lead to reduced energy efficiency and amplified electrode wear. Additionally, the reaction environment in electrochemical NO_x reduction can be acutely harsh, characterized by acidic or alkaline conditions, high temperatures, and high current densities. Consequently, metal alloy electrocatalysts must exhibit stability under such conditions to maintain their catalytic activity over time. Furthermore, the cost of metal alloy electrocatalysts can be a significant factor in the commercial viability of electrochemical NO_x reduction technology. While they are generally less expensive than noble metal catalysts, their lower FE necessitates higher energy consumption. Table 1 highlights the groundbreaking advances in the electrocatalytic performance of metal alloys electrocatalysts.

Metal oxides

Metal oxides have been renowned for their resilience against harsh environments owing to their chemical stability. Numerous studies have demonstrated that NH_3 selectivity exhibits superior performance in acidic conditions compared to neutral or basic ones, making it reasonable to explore the potential of metal

oxides for NO_xRR applications. However, the inert surface and low conductivity of pristine metal oxides have hindered their practical applications. Instead, surface defective metal oxides are energetically more favorable for electrocatalytic applications.

Oxygen vacancies (V_o) are a prevalent type of structural defect in metal oxides, which can significantly impact their electronic and catalytic properties. Therefore, designing metal oxides with an increased density of oxygen defects could be a valuable strategy for optimizing NO_xRR for NH₃ synthesis. For instance, CuO nanocatalysts have been designed with V_o using flame spray pyrolysis (FSP) and mild plasma treatment, resulting in increased V_o amounts linearly correlated to plasma treatment duration.²² The O1s core level spectra analysis via XPS showed the occurrence of V_o with a binding energy of 531.5 eV, whereas EPR measurements revealed the production of ionic superoxide species that resulted from the combination of O₂ molecules and V_o. Defective CuO achieved an NH₃ yield of 520 μmol h⁻¹ cm⁻² at an operating cell voltage of 2.2 V, with over ten operating hours of electrochemical stability in a flow electrolyzer. Undoubtedly, NO_x molecules are captured and activated at the V_o site by bonding with surface Cu atoms and oxygen ions, effectively lowering the binding energy to a remarkable -1.87 eV. The subsequent reduction reaction unequivocally demonstrates that the free energy of most intermediates is significantly lower on the CuO surface with V_o than on the pristine surface.

MnO₂ nanoarrays grown on Ti mesh (MnO_{2-x} NA/TM) have also demonstrated improved NO_xRR performance through the V_o strategy.³² Under the same conditions (0.2 M Na₂SO₄), the catalysts achieved a notable NH₃ yield of 9.9 μmol h⁻¹ cm⁻² with an FE of 82.8%, clearly exceeding the yield and FE of the pristine MnO₂ counterpart (3.2 μmol h⁻¹ cm⁻², 44.8%). This remarkable performance can be attributed to the stronger interaction between NO and Mn atoms induced by the V_o—the less interaction between H and MnO₂ results in high NO_xRR selectivity. Additionally, NO_xRR preferably occurs through an alternating pathway on the MnO_{2-x}(211) surface, with no endothermic steps observed along the reaction pathway. The Ti mesh substrate can also accommodate the growth of other metal oxide nanoarrays, such as NiO nanoarray (NiO NA/TM) catalysts. Such catalysts are highly active and selective for NO_xRR, achieving an NH₃ yield of 125.3 μmol h⁻¹ cm⁻² and an FE of up to 90.0% (see Figure 8).⁹⁸ Metal oxides of distinct morphology have been investigated as potential electrocatalysts for NO_x reduction. For instance, Fe₂O₃ in the form of nanorods has demonstrated exceptional performance, achieving an NH₃ yield of 78.0 μmol h⁻¹ cm⁻² and an FE of 86.7% at -0.4 V.⁹⁹ Meanwhile, TiO₂ nanotubes have exhibited a remarkably high FE of 89.0% at -0.8 V and NH₃ yield of 25.0 μmol h⁻¹ mg_{cat.}⁻¹.¹⁰⁰ Nonetheless, both electrocatalysts generate undesirable byproducts such as H₂ and N₂H₄. Despite the low conductivity limitation of metal oxides, their defective form has outperformed most pristine surface metal oxides. Notwithstanding their attractive cost and abundance, metal oxide electrocatalysts pose significant challenges in the context of electrochemical NO_x reduction. Foremost, metal oxide electrocatalysts often exhibit low electrocatalytic activity, leading to diminished energy efficiency and heightened electrode wear. Furthermore, the selectivity of reduction reactions involving metal oxide electrocatalysts can be challenging to control, resulting in the unwanted formation of products. Table 2 illustrates the latest developments in the electrocatalytic performance of metal oxide electrocatalysts for NO_xRR.

Metal phosphides

Metal phosphides have emerged as an up-and-coming class of electrocatalysts due to their superior conductivity and remarkable stability compared to other transition metal materials. Multifunctional active sites, adjustable structures, and superior stability are the distinguishing characteristics of metal phosphides, which contribute to their electrocatalytic performance comparable to Pt-based materials. Their metal conductor properties and nearly spherical triangular prism element structure offer higher crystal surface exposure, providing more active sites for electrocatalytic processes. The impressive electrocatalytic activity of metal phosphides electrocatalysts is linked to the intrinsic properties of active sites, electron transfer capability, and the number of accessible active sites. In metal phosphides, the phosphorus atoms act as proton acceptors, while the metal atoms serve as hydride acceptors, both of which are crucial active centers. Metal phosphides have proven to be highly versatile electrocatalysts for a variety of reactions, including the HER, OER, ORR, HOR, CO₂RR, NRR, and, most recently, NO_xRR.^{101–103}

In their quest for highly efficient and stable electrocatalysts, researchers have developed cobalt phosphide (CoP) nanowire arrays that are self-supported on carbon cloth for use in the electrocatalytic NO_x⁻ reduction of under ambient conditions in an alkaline NaOH solution.¹⁰⁴ At -0.4 V vs. RHE, the CoP demonstrated a

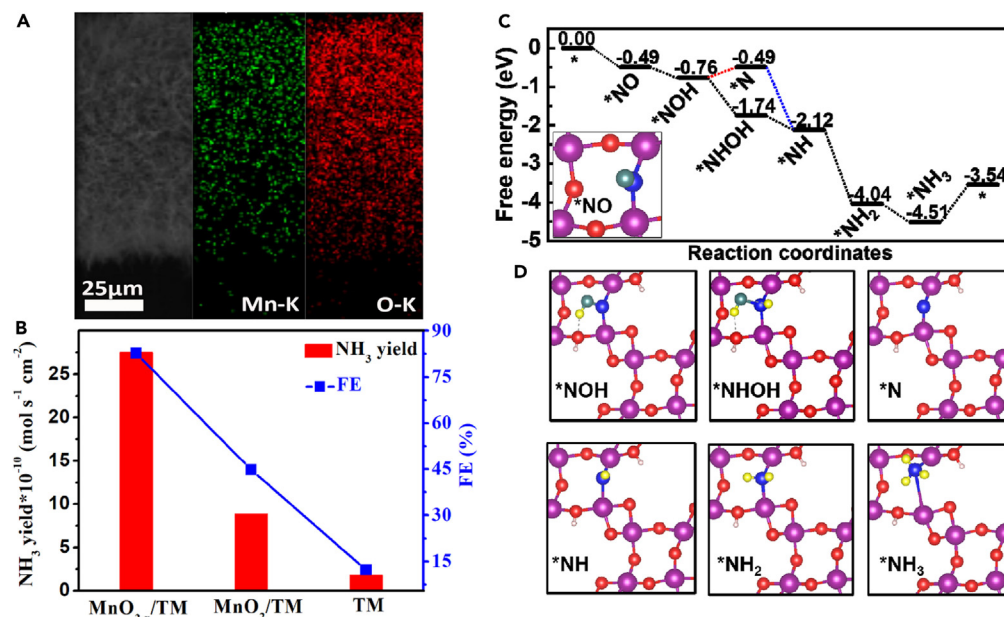


Figure 8. MnO₂ nanoarrays on Ti mesh (MnO_{2-x} NA/TM) for improving NO_xRR performance through the V_o strategy

(A and B) SEM and its corresponding EDX elemental mapping images of MnO_{2-x} nanoarrays grown on Ti mesh (MnO_{2-x} NA/TM) and their (B) corresponding data on NH₃ yields and FEs with different electrodes after bulk electrolysis for an hour at -0.7 V. (C and D) Free energy diagrams of the NO_xRR on MnO_{2-x}(211) along the distal and alternating pathways and (D) the corresponding structures of reaction intermediates. Reprinted with permission from³², Copyright Elsevier Inc 2022.

remarkable NH₃ yield rate of 18.6 μmol h⁻¹ cm⁻² and an FE of 65.0%, maintaining its activity even after ten cycles of electrocatalysis. The exceptional CoP performance is attributed to the charge separation effect within the material, where the Co(δ⁺) → P(δ⁻) mechanism plays a significant role. It significantly enhances the hydrogenation of NO_x⁻ and produces NH₃ selectively by facilitating the adsorption of NO_x⁻ and H atoms on the Co and P sites. Similarly, the use of a nanosheet array of Ni₂P grown on carbon paper (Ni₂P/CP) has demonstrated the provision of a highly selective electrocatalyst for the hydrogenation of NO_x to NH₃, exhibiting a large NH₃ output of 33.5 μmol h⁻¹ cm⁻² and an FE of up to 76.9% at -0.2 V vs. RHE.¹⁰⁵ Based on theoretical calculations, the Ni₂P(111) surface was found to facilitate NO adsorption and activation via an “acceptance-donation” mechanism, with *NO hydrogenation to *NOH identified as the potential-determining step. Researchers have also investigated the feasibility of using FeP electrocatalyst, which demonstrated a low onset potential of -0.014 V and impressive FE of 88.5% with a good generation rate of NH₃ (85.6 μmol h⁻¹ cm⁻²) for the stable electrochemical reduction of NO during an uninterrupted 12-h electrolytic process, as shown in Figures 9B–9D.³⁵ The computer simulation indicated that the adsorbed NO molecules obtained 0.39 e⁻ transferred from the FeP(202) facet (inset in Figure 9A), which showed the electron acceptance and donation phenomenon. The formation of *NH₃ from *NH₂ was identified as the determining factor for the electrocatalytic activity of the FeP(202) facet. Table 2 illustrates the recent advances in the electrocatalytic performance of metal phosphides electrocatalysts for NO_xRR.

To assess the potential of nitrogen-doped BP monolayer-supported transition-metal atoms (MN₃/BP) as NO_xRR electrocatalysts, the study conducted a systematic first-principles calculation of 29 transition-metal atoms. The results showed that MoN₃/BP and IrN₃/BP are the most promising electrocatalysts for NH₃ synthesis, with limiting potentials of -0.10 V and -0.06 V, respectively, comparable to the excellent Pt(111) surface.⁵⁷ The electronic analysis revealed that adsorbed NO species could be activated by hybridizing Mo-4d or Ir-5d orbitals with NO-2p orbitals. Notably, MoN₃/BP and IrN₃/BP exhibit high thermal stability and can be conveniently synthesized utilizing MoCl₃ and IrCl₃ as precursors. Computational simulations have reinforced the potential of metal phosphides as efficient and robust electrocatalysts for NO_xRR and shed light on the reaction mechanism underlying the electroreduction of NO to NH₃ under ambient conditions. The supporting BP monolayer was surprisingly an active NO_xRR electrocatalyst, as it was

Table 2. Electrocatalytic NO_xRR performance of metal oxides, metal phosphides, metal sulfides, metal nitrides, and metal borides

Catalysts	Electrolyte, membrane, cell	NH ₃ yield	FE (%), potential vs. RHE	By product	Reference
MnO ₂ nanoarray	0.2 M Na ₂ SO ₄ , H-type cell, Nafion 117	9.9 μmol h ⁻¹ cm ⁻²	82.8% at -0.7 V	H ₂	Li, et al. ³²
NiO nanosheet array	0.1 M Na ₂ SO ₄ , H-type cell, Nafion 117	125.3 μmol h ⁻¹ cm ⁻²	90% at -0.6 V	-	Liu, et al. ⁹⁸
CuO	0.05 M KNO ₃ + 0.05 M H ₂ SO ₄ , H-type cell, Nafion 117	334.0 μmol h ⁻¹ cm ⁻²	45.0% at -0.7 V	-	Daiyan, et al. ²²
TiO _{2-x}	0.2 M PBS, H-type cell, Nafion 211	72.5 μmol h ⁻¹ cm ⁻²	92.5% at -0.6 V	N ₂ , H ₂	Li, et al. ¹⁰⁸
W/MoO _{3-x}	0.5 M Na ₂ SO ₄ , H-type cell, Nafion 117	308.6 μmol h ⁻¹ cm ⁻²	91.2% at -0.5 V	H ₂ , N ₂ H ₄ , N ₂	Chen, et al. ⁷⁷
Fe ₂ O ₃ nanorods	0.1 M NaOH, H-type cell, Nafion 117	78.0 μmol h ⁻¹ cm ⁻²	86.7% at -0.4 V	H ₂ , N ₂ H ₄	Liang, et al. ⁹⁹
P-doped TiO ₂ nanotubes	0.1 M [C4mpyr][eFAP], H-type cell, Nafion 211	25.0 μmol h ⁻¹ mg _{cat.} ⁻¹	89.0% at -0.8 V	H ₂	Zhang, et al. ¹⁰⁰
Cu NPs/TiO ₂	0.1 M K ₂ SO ₄ , H-type cell, Nafion 117	207.1 μmol h ⁻¹ mg ⁻¹	86.5% at -0.3 V	N ₂ H ₄	Chen, et al. ⁷³
Ni ₂ P nanoarray	0.1 M HCl, H-type cell, Nafion 117	33.5 μmol h ⁻¹ cm ⁻²	76.9% at -0.2 V	N ₂ H ₄ , H ₂	Mou, et al. ¹⁰⁵
FeP nanorod array	0.2 M PBS, three-electrodes cell	14.6 μmol h ⁻¹ cm ⁻²	88.5% at -0.2 V	-	Liang, et al. ³⁵
CoP nanowires	1.0 M NaOH and 2 mM NaNO ₂ , H-type cell, Nafion 117	22.4 μmol h ⁻¹ cm ⁻²	91.6% at -0.3 V	-	Zhang, et al. ¹⁰⁴
CoS nanosheet	0.52 M Na ₂ SO ₄ , H-type cell, Nafion 117	44.7 μmol h ⁻¹ cm ⁻²	53.6% at -0.4 V	H ₂ , N ₂ H ₄	Zhang, et al. ¹⁰⁷
SnS _{2-x} catalyst	0.5 M Na ₂ SO ₄ , H-type cell, Nafion 117	78.6 μmol h ⁻¹ cm ⁻²	90.3% at -0.7 V	H ₂ , N ₂ H ₄ , N ₂	Li, et al. ¹⁰⁹
MoC nanocrystal	0.1 M HCl, H-type cell, Nafion 211	79.4 ± 0.9 μmol h ⁻¹ cm ⁻²	89.0% at -0.8 V	-	Meng, et al. ¹¹⁰
Nanoporous VN	0.1 M HCl, H-type cell, Nafion 211	302.4 μmol h ⁻¹ mg _{cat.} ⁻¹	85.0% at -0.6 V	-	Qi, et al. ¹¹¹
Amorphous NiB ₂	0.5 M Na ₂ SO ₄ , H-type cell, Nafion 117	167.1 μmol h ⁻¹ cm ⁻²	89.6% at -0.4 V	H ₂	Chen, et al. ¹¹²

recently revealed.¹⁰⁶ BP monolayers showed FE of 83.3% at -0.7 V vs. RHE with an NH₃ yield rate of 96.6 μmol h⁻¹ cm⁻². This finding opens a new avenue for metal-free NO_xRR electrocatalysts.

Metal sulfides, metal nitrides, and metal borides

The investigation into metal sulfides, metal nitrides, and metal borides electrocatalysts for the electrochemical reduction of NO_x is a relatively underexplored research area compared to other similar electrocatalytic applications like HER, OER, ORR, and NRR. This could be attributed to various factors, including the intricacy of NO_x reduction, the dearth of suitable metal sulfides, metal nitrides, and metal borides catalysts, and the arduous experimental conditions required to study the electrochemical reduction of NO_x. Nevertheless, the potential advantages of utilizing these electrocatalysts for NO_x reduction make it a promising field of research, which could pave the way to develop more efficient and sustainable methods for mitigating NO_x emissions.

To our knowledge, the CoS nanosheet is the only member of the metal sulfides family examined for electrocatalytic NO_x reduction applications¹⁰⁷—the CoS nanosheets with sulfur vacancies (CoS_{1-x}) have been identified as effective electrocatalysts. In 0.2 M Na₂SO₄ electrolyte, CoS_{1-x} has demonstrated a considerably higher NH₃ yield rate (44.7 μmol h⁻¹ cm⁻²) and FE (53.6%) than the pristine CoS counterpart (27.0 μmol cm⁻² h⁻¹; 36.7%) at a voltage of -0.4 V vs. RHE.¹⁰⁷

In order to investigate the NO reduction mechanism over CoS_{1-x}, DFT was employed. Focusing on the (100) facet of CoS_{1-x}, computational models for CoS(100) and CoS_{1-x}(100) crystal facets were created, and it was found that the NO molecule was adsorbed on both facets due to strong interactions between O atoms in the NO molecule and Co atoms in CoS_{1-x}. In addition, the investigation demonstrated that the initial hydrogenation of NO was the potential determining step (PDS) of NO_xRR on CoS(100) and CoS_{1-x}(100) facets, with corresponding Gibbs free energy barriers of 0.42 and 0.19 eV,¹⁰⁷ respectively. Thus, this study provides crucial information on the possible utilization of transition-metal sulfides with sulfur vacancies for electrochemical NO_x reduction to NH₃.

In the case of metal nitrides, a development has emerged as a nanoporous VN film. This film has been engineered to serve as a NO_xRR electrocatalyst with exceptional selectivity and stability. It achieved a

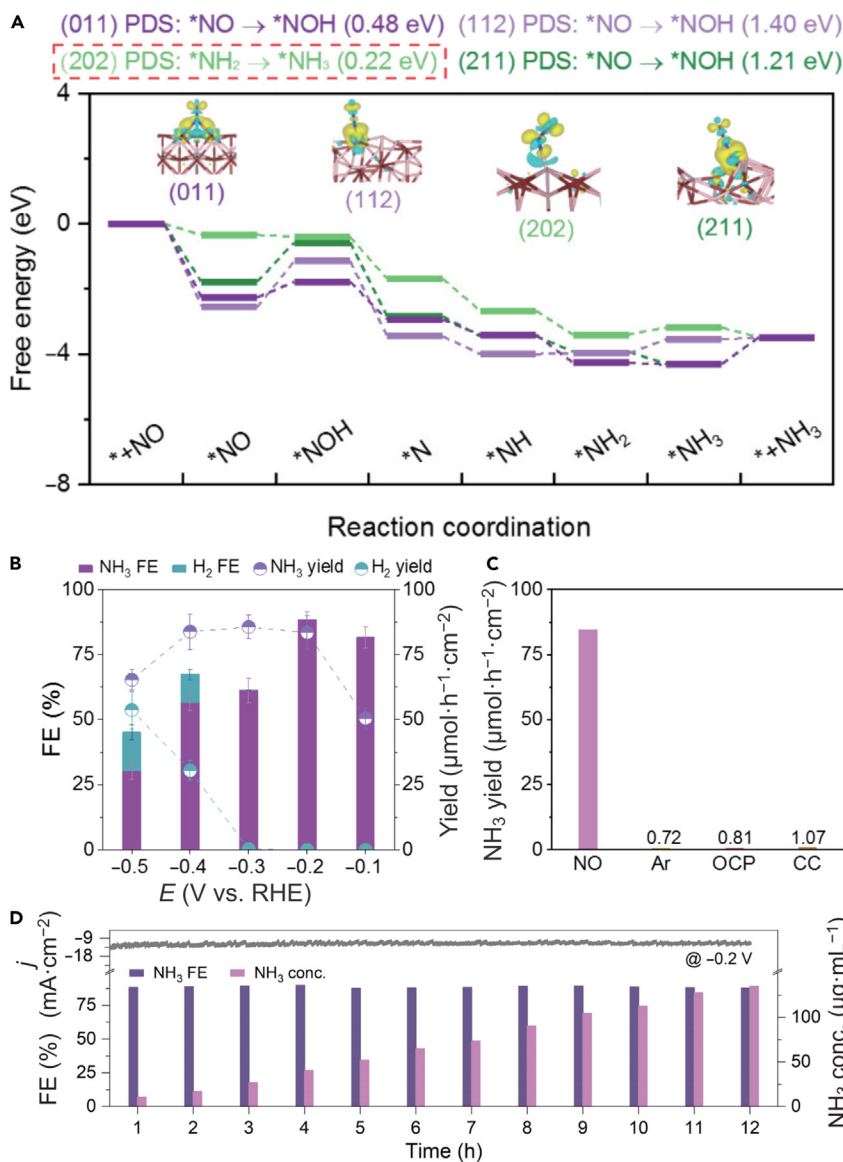


Figure 9. The feasibility of using FeP electrocatalyst for NO_xRR

(A) Free energy diagrams illustrating the electrocatalytic NO_xRR mechanisms occurring on FeP(011), (112), (202), and (211) surfaces, with insets depicting the charge redistribution resulting from NO adsorption. The FeP(202) surface was found to have the lowest free energy barrier for the formation of *NH₃, indicating that the formation of *NH₃ from *NH₂ on this surface was the potential-determining step.

(B and C) Yields and FEs of NH₃ and H₂ obtained on FeP/CC and (C) NH₃ yields obtained using various electrodes under different conditions after bulk electrolysis for an hour.

(D) The long-term stability tests of FeP/CC for NH₃ generation. Reproduced with permission from³⁵, Copyright Springer Nature 2022.

remarkable FE of 85%, accompanied by an NH₃ yield rate of 302.4 μmol h⁻¹ mg_{cat.}⁻¹ at -0.6 V vs. RHE. Moreover, this catalyst demonstrated unparalleled durability, showcasing an outstanding level of sustained activity over a substantial period of 40 h, and maintained negligible current density and minimal decay in the NH₃ yield rate throughout this extended duration. Meanwhile, amorphous NiB₂ catalysts achieved FE of 89.6% with a high NH₃ yield rate at an impressive value of 167.1 μmol h⁻¹ cm⁻². It has been unveiled that the Ni sites within NiB₂ play a pivotal role as the primary active centers. These centers can optimize the binding energy of the crucial *NHO intermediate, reducing energy barriers. Additionally, they exhibit a higher adsorption affinity toward NO than H₂O/H species. This unique characteristic

significantly contributes to facilitating active and selective NORR, enhancing the overall efficiency of the process. Table 2 summarizes the recent advances in the electrocatalytic performance of metal sulfides, metal nitrides, and metal borides electrocatalysts for NO_xRR.

Overall, there has been extensive exploration of various electrocatalysts for NO_xRR. Some have demonstrated high NH₃ yield but require operation at high voltage, resulting in substantial electrical energy consumption and, subsequently, high NH₃ prices. Conversely, although high FE is observed when operated at low voltage, the NH₃ yield rate may not meet industrial requirements. In this context, researchers need to develop highly active catalysts that exhibit both high FE at low operating voltage and satisfactory NH₃ yield rates. We present the comprehensive performance metrics (NH₃ yield rate, FE, and operating voltage) of selected catalysts in Figure 10.

BEYOND ELECTROCATALYSTS DESIGN

While much attention has been focused on electrocatalyst design for NO_xRR, there is a need to go beyond this and explore other factors that can enhance the electrochemical performance of NO_xRR. This includes modifications to the electrolyte and gas diffusion electrode (GDE) design, which can significantly impact the reaction efficiency. By noting these aspects, it may be possible to develop more efficient and sustainable methods for NO_xRR, which could ultimately lead to a reduction in NO_x emissions. This chapter will explore various strategies and techniques beyond electrocatalyst design for enhancing the electrochemical NO_xRR process. We will discuss the modification of electrolytes to improve reaction kinetics and the design of GDEs to optimize mass transfer. Additionally, we will delve into the proof-of-concept of Zn-NO batteries and the integration of highly active electrocatalysts as cathode materials into the battery architecture for improved performance. This chapter aims to provide a comprehensive overview of the latest developments and challenges in NO_xRR enhancement beyond electrocatalyst design.

Electrolytes modification

Utilizing NO_x gas directly from the atmosphere presents a new opportunity for transforming waste into valuable chemicals. However, capturing and concentrating NO_x from polluted air demands sophisticated infrastructure, which may hinder the practical application of this approach. Additionally, the inadequate solubility of NO_x gas in aqueous electrolytes, predominantly the NO molecule, hinders the mass transfer and creates an unfavorable surrounding for the electrochemical conversion of NO_x. Overcoming these challenges has become a major focus of research in the field of electrochemical reduction of NO_x. This section will discuss the latest advancements in developing deliberately designed electrolytes aimed at fully optimizing NO_xRR.

Producing NH₃ via NO_xRR offers significant advantages compared to NRR and Haber-Bosch methods, which rely on inert N₂ as a resource. However, achieving high conversion rates of NO_x through electroreduction is limited by the intrinsically low solubility of NO (~1.94 mM at 25°C) in water. In electrochemical reduction processes like NRR and CO₂RR, the choice of electrolytes as gas-dissolving media is critical. For example, electrolyte design has enabled high selectivity in the electroreduction of CO₂ into targeted chemicals. Similarly, to achieve higher conversion rates and improved selectivity in electrocatalytic NO_xRR, strategic control over the gas solubility and fine-tuning the electrochemical processes occurring at the interface of the electrode and electrolyte are vital. With a meticulous approach, the performance of electrocatalytic reactions can be significantly enhanced, leading to remarkable gains in efficiency and productivity.

EDTA–Fe²⁺ metal complex (EFeMC) is a well-known compound that can capture NO_x rapidly. The ligands within EFeMC provide a favorable environment to prevent Fe precipitation, a major adsorption site for NO, and to stabilize the adsorbed-NO on a metal complex (NO@EFeMC). It is expected that EFeMC increases the solubility of NO in aqueous electrolytes. Kim et al.¹¹³ have recently unveiled a critical contribution of EFeMC in the selective reduction of NO for efficient NH₃ production. The electrochemical reduction of NO in phosphate-buffered saline (PBS) electrolyte with the presence of EFeMC additives is diffusion-controlled because charges are taken from the electrode via an outer-sphere electron transfer of the Helmholtz plane where the NO@EFeMC species exist. This has led to nearly 100% efficiency for NH₃ with a current density of 50 mA cm⁻² at -0.165 V vs. RHE and negligible catalytic degradation for up to 120 h. Without EFeMC additives (or only PBS), the N₂O molecule was a dominant product at low overpotential, indicating that N–N dimerization (N₂O formation) favorably occurs in a more accessible free NO molecules

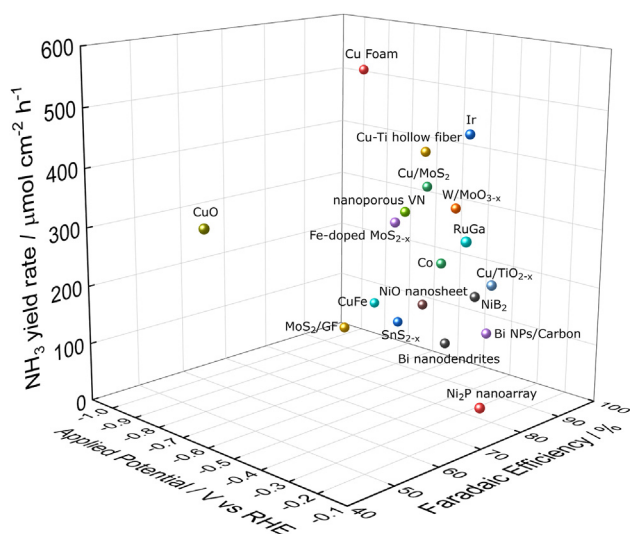


Figure 10. Overall performances of selected NO_xRR electrocatalysts

environment, in line with the previous report.¹¹⁴ Such dimerization is less possible in PBS electrolytes containing EFeMC additive because the accessibility to free NO molecules is unavailable. However, the conversion efficiency decreased in a highly concentrated NO gas due to its desorption from EFeMC that may react with other species, such as NH₃OH⁺, forming an N₂O molecule. From a complementary computational study, the EDTA ligand is involved in the electron transfer process, providing favorable reaction-free energy and stabilizing the rate-limiting *HNO intermediate through H-bond formation. Ferrous-based electrolyte such as ferric chelate has been used to enhance NO conversion yield of 14.6 μmol h⁻¹ cm⁻² at -0.1 V with FE of 65.2%.²⁵ The wide choice of additives will allow for tailoring the electrolytes toward the most favorable conditions for the electrochemical reduction of NO_x to NH₃.

Ferrous chelate can also be a promising electrolyte to drive the NO_xRR because it acts as an effective electrolyte for NO_x absorption in the NO_xRR process based on the brown-ring reaction. Ferrous chelate can be fully reduced at a lower onset potential on rGO (reduced graphene oxide) electrode, allowing continuous NO_x reduction. Additionally, ferrous chelate can be regenerated for reuse, making it a sustainable option for NO_xRR.²⁵ The application of ferrous chelate circumvents the influence of EDTA on NH₃ detection and facilitates the two-phase transition from Fe^{II}(NO)Cit to NH₃. By reducing ferrous iron by coordination reaction, the potential associated with the HER and NO_xRR is lowered, enabling selective activation of coordinated NO_x in the ferrous electrolyte by the Au catalyst while preventing the reduction of ferrous to iron under relevant potentials.

Despite being a good capturer for NO_x, the presence of metal complexes as electrolyte additives may need to be more friendly for producing high-purity NH₃. Alternatively, Krzywda et al.⁸⁹ performed electrochemical reduction of NO_x in different electrolytes (H₂SO₄, HClO₄, and Na₂SO₄) without additives in an attempt to solve the low solubility and limited mass transfers of the NO_x. They found that NH₃ and H₂ were preferably formed in an acidic environment, while N₂O and N₂ existed in copious quantities at neutral electrolytes. In acidic electrolytes, the occurrence of HER is high because the requirement of the water dissociation step is fulfilled, which allows the transformation of NH₄⁺ to NH₃ during the scan direction toward positive potential. In neutral electrolytes, HER is kinetically sluggish and suppressed, thus increasing the chance of NO with OH⁻ interaction with subsequent formation of N₂O, N₂, or NO₂⁻/NO₃⁻ species. This work showed a positive indication that electrochemical reduction of NO_x could be performed in additives-free electrolytes.

Design of gas diffusion electrode (GDE)

Besides the importance of electrolyte choice, electrode configuration and design may overcome the limitation of NO_x. A GDE is an electrode that allows a gas to diffuse through it and react with a liquid electrolyte. The GDE consists of three distinctive layers, namely the gas diffusion layer (GDL), catalyst layer (CL), and microporous layer (MPL), which serves as a barrier between the GDL and CL, and are essential

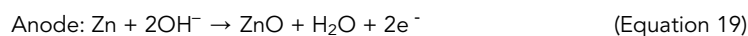
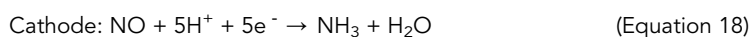
components in the construction of the electrode.¹¹⁵ The GDL allows the gas to diffuse uniformly and provides electrical conductivity, while the CL contains the active catalyst particles that facilitate the electrochemical reaction. The MPL enhances the gas transport and prevents the electrolyte from flooding the GDL. GDEs have been utilized for various electrochemical processes, such as CO₂RR and NRR. Cheon et al.¹¹⁶ presented a new approach to converting NO to NH₃ using a GDE. The reaction mechanism involves several steps, including (1) NO gas diffuses through the GDE and reaches the catalyst layer, where it is adsorbed and reduced to nitroxyl (HNO) by electrons from the external circuit; (2) HNO reacts with water to form nitrous acid (HNO₂) and hydroxide ions (OH⁻); (3) HNO₂ is further reduced to NO₂⁻ and protons (H⁺); (4) NO₂⁻ reacts with water to form nitric acid (HNO₃) and OH⁻; (5) HNO₃ is reduced to NH₃ and O₂ at the catalyst surface; and (6) NH₃ dissolves in the electrolyte and diffuses out of the GDE, while O₂ gas bubbles out of the electrode. This method offers a more convenient and cost-effective means of handling and storing NO, as dilute NO (0.1%) can be used instead of concentrated NO (10%). The GDE also provides improved mass transport and reaction kinetics for NO electroreduction, leading to high production rates of NH₃ (up to 2.4 mmol h⁻¹ cm⁻²) with high selectivity (up to 95%).

Cu foam is a conventional GDE for electrochemical reduction of N₂ or NO_x, which gives a high NH₃ production rate with a decent FE > 90.0%. However, Cu foam electrodes are not sustained in acidic conditions, which impacts their long-standing use. Correspondingly, researchers developed a Cu-Ti hollow fiber electrode as a non-traditional electrode geometry to combat NO_x mass transport limitations and enhance electrode stability in low pH environments.⁸⁹ In a feed gas containing 10% of NO, NH₃ production rates of 400 μmol h⁻¹ cm⁻² with FE of almost 90.0% were achieved in neutral electrolytes at -0.6 V vs. RHE, improving the practical ability of the flow cell system configuration. It will also be relevant when seeing NO_x waste from the combustion process as a NO_x source. However, the high NH₃ production rate and FE emphasized in this work can still not compete with the state-of-the-art HB process, which requires 10 kWh kg⁻¹ of NH₃. This work has paved the way for using flow-through hollow fiber electrode configuration and low concentration of NO feeding while maintaining a high conversion rate regardless.

While GDE is critical for scaling up NO_x electrocatalysis, the catalyst requirements may differ from those of h-type electrochemical cells. In a typical GDE, the flow of electrolytes containing saturated NO_x needs to be continuously supplied to the catholyte to promote NO_x reduction. In this regard, the mechanical shear may corrode and diminish the catalyst layer after some time. Therefore, a strong attachment between catalysts or the catalyst and current collector is necessary to prevent a decrease in the catalyst amount during the extended operating hours of catholyte flows. Additionally, the catalysts should rapidly capture and activate the NO_x molecules in the catholyte due to this flow, ensuring effective conversion into NH₃.

NO_xRR electrocatalysts as cathode materials in Zn-NO batteries

The Zn-NO battery is a redox flow battery that employs Zn and NO as the active redox species and is operated in an H-type configuration. Within this arrangement, the cathodes, containing catalysts, are located in a cathodic electrolyte, which could either be a neutral or acidic solution. Meanwhile, an anodic electrolyte with a polished zinc plate is immersed in 1 M KOH or NaOH. A bipolar membrane separates these two electrolytes. The Zn-NO battery has gained significant attention due to its potential for high energy density, cost-effectiveness, and eco-friendliness. It is a proof-of-concept of achieving three goals at once, including NO elimination, sustainable NH₃ production, and electrical energy output. The performance of Zn-NO is characterized by two parameters; power density (mW cm⁻²) and NH₃ yield (μmol h⁻¹ mg_{cat.}⁻¹) it delivers. This subchapter will discuss the mechanisms of storage and conversion, recent developments in cathode materials, and the limitations and challenges associated with Zn-NO batteries. The storage and conversion mechanisms of the batteries rely on reversible redox reactions between Zn and NO, and the electrochemical processes taking place at each electrode can be elucidated as follows during the charging-discharging cycle:



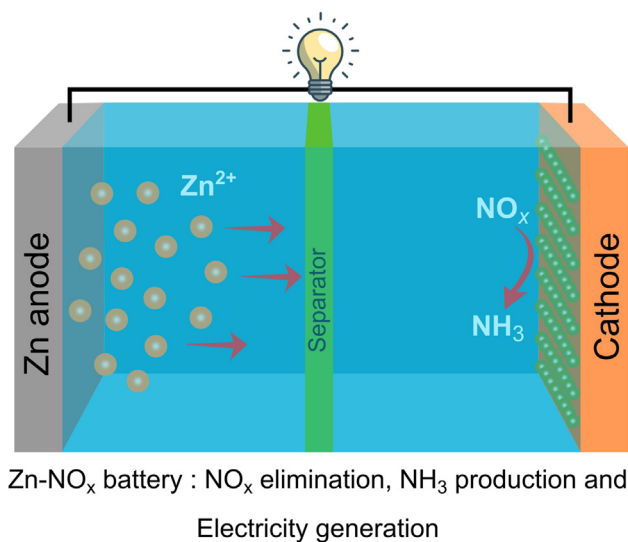
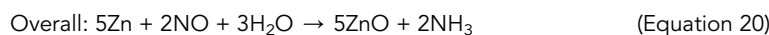


Figure 11. Zn-NO_x battery structures and working mechanism



The materials used in Zn-NO batteries are critical for their performance and durability. The negative half-cell typically uses a Zn-based electroactive material at which, so far, only a polished Zn plate has been reported. The positive half-cell typically uses a NO_xRR catalyst to reduce NO_x to NH₃, as shown in Figure 11. These materials must be carefully chosen to ensure high efficiency, stability, and safety in the Zn-NO system.

Several previously discussed electrocatalysts have been employed as cathode materials in Zn-NO batteries, and some have demonstrated a remarkably long-lasting performance. These electrocatalysts have been observed to play a crucial role in improving the efficiency and stability of the battery by enhancing the conversion of nitrate ions into nitrite ions. This has resulted in better performance and increased durability of the batteries, making them more practical for various applications. The performances of NO_xRR electrocatalyst cathode in Zn-NO battery are compiled in Table 3.

There are generally several limitations and challenges associated with Zn-NO batteries. One of the main challenges is the low solubility of NO in most electrolytes, which limits the amount of NO that can be stored in the positive half-cell and reduces the overall energy density of the battery. Another challenge is the low conductivity of NO, which can reduce the rate at which the redox reactions occur and limit the battery's power density. Additionally, the corrosion of Zn and the instability of NO under certain conditions can also affect the performance and durability of Zn-NO batteries. For example, the exposure of Zn to O₂ or water can cause corrosion, while the exposure of NO to water or high temperatures can cause decomposition. These issues must be carefully addressed to ensure the long-term stability and reliability of Zn-NO batteries. Overall, Zn-NO batteries have the potential to provide a high-energy, low-cost, and environmentally friendly alternative to conventional batteries. However, further research is needed to overcome the challenges associated with their storage and conversion mechanisms, materials, and stability.

CONCLUSION AND OUTLOOK

In summation, this review offers an extensive overview of the recent advancements in the application of electrochemical reduction for toxic NO_x gas elimination. Electrochemical reduction presents an attractive option for NO_x remediation in the air, as it boasts exceptional properties such as high efficiency, lack of secondary pollutants, and environmental friendliness. The triumph of electrochemical NO_x reduction hinges on the quality of electrode materials employed. Therefore, a diverse range of electrocatalysts, including SACs, 2D materials, metal oxides, metal phosphides, molecular catalysts, etc., have been extensively studied, both computationally and experimentally, for their remarkable electrochemical performance and cost-effectiveness. Extensive progress has been made in exploring electrolyte additives and

Table 3. Performance of the NO_xRR electrocatalysts as a cathode in Zn-NO battery

Electrocatalysts	Power density	NH ₃ yield	Reference
MoC	1.80 mW cm ⁻²	57.5 μmol h ⁻¹ mg _{cat.} ⁻¹ at 0.5 mA cm ⁻²	Meng, et al. ¹¹⁰
TiO _{2-x}	0.84 mW cm ⁻²	14.2 μmol h ⁻¹ cm ⁻²	Li, et al. ¹⁰⁸
NiO	0.88 mW cm ⁻²	13.4 μmol h ⁻¹ cm ⁻²	Liu, et al. ⁹⁸
MoS ₂ nanosheet	1.04 mW cm ⁻²	24.2 μmol h ⁻¹ mg _{cat.} ⁻¹	Zhang, et al. ³⁴
Ni ₂ P	1.53 mW cm ⁻²	3.7 μmol h ⁻¹ mg _{cat.} ⁻¹	Mou, et al. ¹⁰⁵
Binanoparticles/carbon nanosheet	2.35 mW cm ⁻²	20.9 μmol h ⁻¹ mg _{cat.} ⁻¹	Liu, et al. ⁷⁵
Binanodendrites	2.33 mW cm ⁻²	5.0 μmol h ⁻¹ cm ⁻²	Lin, et al. ⁹²
NiFe layered double hydroxide	1.80 mW cm ⁻²	32.0 μmol h ⁻¹ cm ⁻²	Meng, et al. ¹¹⁷
Single atomic Ce	3.40 mW cm ⁻²	18.2 μmol h ⁻¹ mg _{cat.} ⁻¹	Zhang, et al. ¹¹⁸
Fe ₂ O ₃ nanorod	1.18 mW cm ⁻²	8.5 μmol h ⁻¹ mg _{cat.} ⁻¹	Liang, et al. ⁹⁹
CoS _{1-x} nanosheet	2.06 mW cm ⁻²	87.8 μmol h ⁻¹ mg _{cat.} ⁻¹	Zhang, et al. ¹⁰⁷
CoP nanoarray	0.496 mW cm ⁻²	16.8 μmol h ⁻¹ mg _{cat.} ⁻¹	Liang, et al. ¹¹⁹
Hexagonal Co nanosheets	4.66 mW cm ⁻²	14.6 μmol h ⁻¹ mg _{cat.} ⁻¹	Wang, et al. ¹²⁰

GDE concerning NO_x electroreduction. The potential of NO_x electroreduction catalysts as a Zn-NO_x battery cathode has additionally proven crucial in NO_x abatement, environmentally friendly NH₃ production, and electricity generation. Nevertheless, unresolved challenges, as listed below, necessitate further research and development.

- (1) The reduction of NO_x has been the subject of extensive research; however, the detailed mechanism is still uncertain due to the complex multiple electron-proton transfers and instability of intermediates. Although DFT calculations and MD simulations are valuable tools, they may only partially replicate the complex and dynamic electrochemical reaction process under realistic circumstances. To establish an optimal electrochemical system, developing a range of *in situ* electrochemical characterization methods is crucial to clarify the reaction intermediates, reaction pathways, final products, and structure-activity relationships (SARs).
- (2) Most NO_x research centers on electrochemical reduction, where NH₃ selectivity can reach nearly 80%. Other methods, such as photocatalysis, thermal catalysis, and photoelectrochemical processes, may prove promising for NO_x treatment in the future. These methods offer the potential for cost-effectiveness due to the direct utilization of almost infinite solar energy to drive catalytic processes. For example, solar water splitting and CO₂ conversion into fuels have been successfully tested. Therefore, there is an opportunity for solar conversion of NO_x into NH₃.
- (3) Metallic electrodes, mainly in the single-atom form, are the backbone of the electrochemical reduction of NO_x, owing to their nearly full atomic utilization and remarkable catalytic activity resulting from a low-coordination surrounding and a greater number of accessible active sites. Nonetheless, these electrocatalysts are susceptible to oxidative dissolution, surface poisoning, and leaching, which can diminish their electrochemical activity and pose environmental hazards. Additionally, typical experiments only evaluate their performance over a few hours, which needs to be improved for industrial application or to compete with the current Haber-Bosch process. Hence, developing highly stable electrocatalysts capable of maintaining their performance for more than 1000 h is essential to realize the goal of transforming waste into valuable resources. Apart from stability, the cathode materials' activity and selectivity should also be emphasized more in practical applications.
- (4) The conundrum of NO_x solubility in aqueous solutions calls for an immediate resolution. One viable approach to this predicament involves the exploration of electrolytes, such as ionic liquids, which potentially enhance the solubility of NO_x and augment the ionic conductivity of the electrochemical system as a whole. In addition, optimizing the GDE should be pursued with fervor to enable the continuous generation of NH₃ from NO_x. Further research is needed to fully explore these techniques' potential and develop innovative solutions to tackle the challenges of NO_x solubility in aqueous solutions.

- (5) Enhancing the efficiency of NO_x mass transfer and maximizing NO_x concentration on the catalyst surface are critical aspects of the structural design of a GDE-type electrolyzer. These optimizations enable the attainment of industrial-grade current density and superior electroreduction performance. However, to allow the large-scale application of NO_x electrocatalysts in the future, it is essential to improve their stability. This necessitates the development of catalyst materials with enhanced performance, long-term stability, and reduced cost. Additionally, addressing challenges such as electrolyte flooding and inorganic salt crystallization in GDE systems is crucial. To overcome these obstacles, explore superhydrophobic materials and utilize emerging ionic liquid-based electrolytes. By tackling these issues, it becomes possible further to optimize the performance and durability of GDE-type electrolyzers, paving the way for their widespread implementation.
- (6) The selectivity of certain NO_xRR catalysts may remain relatively low, resulting in less-than-optimal energy efficiency, often below 50%. While there is some value in the by-products of H₂ and N₂H₄, their actual usefulness depends on various factors, including scale and geographic location. Unfortunately, NO_xRR typically requires more negative potentials than normal HER (at equivalent partial current densities). Consequently, the production of H₂ products during NO_xRR comes at a significantly higher energy cost than in practical water electrolysis.
- (7) The utilization of NO_x electrocatalysts in the cathode of a Zn-NO_x battery represents a remarkable demonstration of the synergy between the eradication of NO_x, NH₃ synthesis, and electricity generation. Nevertheless, the implementation of this technology faces hurdles, such as the non-rechargeable nature of Zn-NO_x, attributed to the limited activity of NO_x catalysts to undergo the OER during the charging process. To surmount this challenge, efforts should be directed toward exploring innovative cathode materials with bifunctionality for both NO_xRR and OER so that Zn-NO_x can be charged and discharged.
- (8) As the generic system works at aqueous conditions, the environmental concerns induced by ammonium in the solution should be strictly considered. Ammonium has various effects depending on the specific circumstances and the system's chemistry. The primary concern is that ammonium is potentially toxic and difficult to handle once converted to nitrate (NO₃⁻) and nitrite (NO₂⁻). Therefore, the operating parameters should be valued carefully to prevent the associated issues and ensure proper operations.
- (9) When evaluating the feasibility and sustainability of the electrochemical reduction of NO_x, life cycle assessment can help quantify the environmental impact of the entire process, from raw material extraction to end-of-life disposal, and identify areas for improvement. Techno-economic analysis, on the other hand, can evaluate the economic viability of the process and identify ways to reduce production costs. By noting both environmental and economic factors, the development of electrochemical NO_x reduction technologies can be optimized for maximum sustainability and commercialization potential.

ACKNOWLEDGMENTS

A.H. acknowledges the financial support from The Indonesia Endowment Funds for Education and National Research and Innovation Agency under Riset dan Inovasi untuk Indonesia Maju (RIIM) with grant number 82/II.7/HK/2022. V.N.A. acknowledges support from the Japan Society for the Promotion of Science (JSPS) through a Grant-in-Aid for a Research Activity Start-up (No. 21K21329). Z.W.S. acknowledges the Agency for Science, Technology and Research (Central Research Fund Award).

DECLARATION OF INTERESTS

The authors state that there are no financial interests or personal relationships that could have potentially affected the work reported in this paper.

REFERENCES

1. Brunekreef, B., and Holgate, S.T. (2002). Air pollution and health. *Lancet* 360, 1233–1242. [https://doi.org/10.1016/S0140-6736\(02\)11274-8](https://doi.org/10.1016/S0140-6736(02)11274-8).
2. Lelieveld, J., Evans, J.S., Fnais, M., Giannadaki, D., and Pozzer, A. (2015). The contribution of outdoor air pollution sources to premature mortality on a global scale. *Nature* 525, 367–371. <https://doi.org/10.1038/nature15371>.
3. India State-Level Disease Burden Initiative Air Pollution Collaborators, Dey, S., Gupta, T., Dhaliwal, R.S., Brauer, M., Cohen, A.J., Stanaway, J.D., Beig, G., Joshi, T.K., Aggarwal, A.N., et al. (2019). The impact of air pollution on deaths, disease burden, and life expectancy across the states of India: the Global Burden of Disease Study 2017. *Lancet Planet. Health* 3, e26–e39. [https://doi.org/10.1016/S2542-5196\(18\)30261-4](https://doi.org/10.1016/S2542-5196(18)30261-4).
4. Vallero, D. (2014). The Science of Air Pollution. In *Fundamentals of Air Pollution* (Elsevier), pp. 43–81. <https://doi.org/10.1016/B978-0-12-401733-7.00003-7>.
5. Bai, X., Chen, H., and Oliver, B.G. (2022). The health effects of traffic-related air pollution: A review focused the health effects of going green. *Chemosphere* 289, 133082. <https://doi.org/10.1016/j.chemosphere.2021.133082>.

6. Kampa, M., and Castanas, E. (2008). Human health effects of air pollution. *Environ. Pollut.* *151*, 362–367. <https://doi.org/10.1016/j.envpol.2007.06.012>.
7. Williams, P.B., Alexis, N., Barnes, C., Bernstein, I.L., Bernstein, J.A., Nel, A., Peden, D., Diaz-Sanchez, D., Tarlo, S.M., and Bernstein, J.A. (2004). Health effects of air pollution. *J. Allergy Clin. Immunol.* *114*, 1116–1123. <https://doi.org/10.1016/j.jaci.2004.08.030>.
8. Choma, E.F., Evans, J.S., Gómez-Ibáñez, J.A., Di, Q., Schwartz, J.D., Hammit, J.K., and Spengler, J.D. (2021). Health benefits of decreases in on-road transportation emissions in the United States from 2008 to 2017. *Proc. Natl. Acad. Sci. USA* *118*. e2107402118. <https://doi.org/10.1073/pnas.2107402118>.
9. Masera, K., and Hossain, A.K. (2023). Advancement of biodiesel fuel quality and NOx emission control techniques. *Renew. Sustain. Energy Rev.* *178*, 113235. <https://doi.org/10.1016/j.rser.2023.113235>.
10. Mohd Shafie, S.H., and Mahmud, M. (2020). Urban Air Pollutant from Motor Vehicle Emissions in Kuala Lumpur, Malaysia. *Aerosol Air Qual. Res.* *20*, 2793–2804. <https://doi.org/10.4209/aaqr.2020.02.0074>.
11. Sarfraz, M. (2021). Green Technologies to Combat Air Pollution, pp. 143–161. https://doi.org/10.1007/978-3-030-70509-1_9.
12. Wang, S., and Hao, J. (2012). Air quality management in China: Issues, challenges, and options. *J. Environ. Sci.* *24*, 2–13. [https://doi.org/10.1016/S1001-0742\(11\)60724-9](https://doi.org/10.1016/S1001-0742(11)60724-9).
13. Xu, W., Xie, Y., Xia, D., Ji, L., and Huang, G. (2022). Visualizing invisible NOx emissions and remodeling policy requirements within bidirectional supply-demand control. *J. Clean. Prod.* *380*, 134915. <https://doi.org/10.1016/j.jclepro.2022.134915>.
14. Erisman, J.W., Sutton, M.A., Galloway, J., Klimont, Z., and Winiwarter, W. (2008). How a century of ammonia synthesis changed the world. *Nat. Geosci.* *1*, 636–639. <https://doi.org/10.1038/ngeo325>.
15. Klerke, A., Christensen, C.H., Nørskov, J.K., and Vegge, T. (2008). Ammonia for hydrogen storage: challenges and opportunities. *J. Mater. Chem.* *18*, 2304. <https://doi.org/10.1039/b720020j>.
16. Kitano, M., Inoue, Y., Yamazaki, Y., Hayashi, F., Kanbara, S., Matsuiishi, S., Yokoyama, T., Kim, S.-W., Hara, M., and Hosono, H. (2012). Ammonia synthesis using a stable electride as an electron donor and reversible hydrogen store. *Nat. Chem.* *4*, 934–940. <https://doi.org/10.1038/nchem.1476>.
17. Amrillah, T., Hermawan, A., Alviani, V.N., Seh, Z.W., and Yin, S. (2021). MXenes and their derivatives as nitrogen reduction reaction catalysts: recent progress and perspectives. *Mater. Today Energy* *22*, 100864. <https://doi.org/10.1016/j.mtener.2021.100864>.
18. Guo, X., Du, H., Qu, F., and Li, J. (2019). Recent progress in electrocatalytic nitrogen reduction. *J. Mater. Chem.* *7*, 3531–3543. <https://doi.org/10.1039/C8TA11201K>.
19. Foster, S.L., Bakovic, S.I.P., Duda, R.D., Maheshwari, S., Milton, R.D., Minter, S.D., Janik, M.J., Renner, J.N., and Greenlee, L.F. (2018). Catalysts for nitrogen reduction to ammonia. *Nat. Catal.* *1*, 490–500. <https://doi.org/10.1038/s41929-018-0092-7>.
20. Smith, C., Hill, A.K., and Torrente-Murciano, L. (2020). Current and future role of Haber-Bosch ammonia in a carbon-free energy landscape. *Energy Environ. Sci.* *13*, 331–344. <https://doi.org/10.1039/C9EE02873K>.
21. Hermawan, A., Amrillah, T., Alviani, V.N., Raharjo, J., Seh, Z.W., and Tsuchiya, N. (2023). Upcycling air pollutants to fuels and chemicals via electrochemical reduction technology. *J. Environ. Manag.* *334*, 117477. <https://doi.org/10.1016/j.jenvman.2023.117477>.
22. Daiyan, R., Tran-Phu, T., Kumar, P., Iputera, K., Tong, Z., Leverett, J., Khan, M.H.A., Asghar Esmailpour, A., Jalili, A., Lim, M., et al. (2021). Nitrate reduction to ammonium: From CuO defect engineering to waste NOx-to-NH3 economic feasibility. *Energy Environ. Sci.* *14*, 3588–3598. <https://doi.org/10.1039/d1ee00594d>.
23. Wan, H., Bagger, A., and Rossmel, J. (2021). Electrochemical Nitric Oxide Reduction on Metal Surfaces. *Angew Chem. Int. Ed. Engl.* *60*, 21966–21972. <https://doi.org/10.1002/anie.202108575>.
24. Soto-Hernández, J., Santiago-Ramirez, C.R., Ramirez-Meneses, E., Luna-Trujillo, M., Wang, J.A., Lartundo-Rojas, L., and Manzo-Robledo, A. (2019). Electrochemical reduction of NOx species at the interface of nanostructured Pd and PdCu catalysts in alkaline conditions. *Appl. Catal. B Environ.* *259*, 118048. <https://doi.org/10.1016/j.apcatb.2019.118048>.
25. Xiong, Y., Li, Y., Wan, S., Yu, Y., Zhang, S., and Zhong, Q. (2022). Ferrous-based electrolyte for simultaneous NO absorption and electroreduction to NH3 using Au/rGO electrode. *J. Hazard Mater.* *430*, 128451. <https://doi.org/10.1016/j.jhazmat.2022.128451>.
26. Long, J., Chen, S., Zhang, Y., Guo, C., Fu, X., Deng, D., and Xiao, J. (2020). Direct Electrochemical Ammonia Synthesis from Nitric Oxide. *Angew Chem. Int. Ed. Engl.* *59*, 9711–9718. <https://doi.org/10.1002/anie.202002337>.
27. Lin, C.-Y., Hung, W.-T., Wu, C.-T., and Ho, K.-C. (2009). Electrochemical reduction of NO2 at a Pt/membrane electrode—Application to amperometric NO2 sensing. *Sensor. Actuator. B Chem.* *136*, 32–38. <https://doi.org/10.1016/j.snb.2008.10.049>.
28. KUWABATA, S., and NAKAGAWA, M. (2002). Electrochemical Reduction of NO, NO₂⁻, and NO₃⁻ using Prussian Blue Film-coated Electrode. *Electrochemistry* *70*, 855–859. <https://doi.org/10.5796/electrochemistry.70.855>.
29. Hao, R., Tian, L., Wang, C., Wang, L., Liu, Y., Wang, G., Li, W., and Ozin, G.A. (2022). Pollution to solution: A universal electrocatalyst for reduction of all NOx-based species to NH3. *Chem Catal.* *2*, 622–638. <https://doi.org/10.1016/j.checat.2022.01.022>.
30. Merino, L., Örnemark, U., and Toldrá, F. (2017). Analysis of nitrite and nitrate in foods: overview of chemical, regulatory and analytical aspects. *Adv. Food Nutr. Res.* *81*, 65–107. <https://doi.org/10.1016/bs.afnr.2016.11.004>.
31. Kim, D.H., Ringe, S., Kim, H., Kim, S., Kim, B., Bae, G., Oh, H.-S., Jaouen, F., Kim, W., Kim, H., and Choi, C.H. (2021). Selective electrochemical reduction of nitric oxide to hydroxylamine by atomically dispersed iron catalyst. *Nat. Commun.* *12*, 1856. <https://doi.org/10.1038/s41467-021-22147-7>.
32. Li, Z., Ma, Z., Liang, J., Ren, Y., Li, T., Xu, S., Liu, Q., Li, N., Tang, B., Liu, Y., et al. (2022). MnO₂ nanorod with oxygen vacancies: An efficient catalyst for NO electroreduction to NH₃ at ambient conditions. *Mater. Today Phys.* *22*, 100586. <https://doi.org/10.1016/j.mtphys.2021.100586>.
33. Foral, M.J., and Langer, S.H. (1991). Sulfur coverage effects on the reduction of dilute nitric oxide at platinum black gas diffusion electrodes. *Electrochim. Acta* *36*, 299–307. [https://doi.org/10.1016/0013-4686\(91\)85253-4](https://doi.org/10.1016/0013-4686(91)85253-4).
34. Zhang, L., Liang, J., Wang, Y., Mou, T., Lin, Y., Yue, L., Li, T., Liu, Q., Luo, Y., Li, N., et al. (2021). High-Performance Electrochemical NO Reduction into NH₃ by MoS₂ Nanosheet. *Angew Chem. Int. Ed. Engl.* *60*, 25263–25268. <https://doi.org/10.1002/anie.202110879>.
35. Liang, J., Zhou, Q., Mou, T., Chen, H., Yue, L., Luo, Y., Liu, Q., Hamdy, M.S., Alshehri, A.A., Gong, F., and Sun, X. (2022). FeP nanorod array: A high-efficiency catalyst for electroreduction of NO to NH₃ under ambient conditions. *Nano Res.* *15*, 4008–4013. <https://doi.org/10.1007/s12274-022-4174-0>.
36. Andana, T., Rappé, K.G., Gao, F., Szanyi, J., Pereira-Hernandez, X., and Wang, Y. (2021). Recent advances in hybrid metal oxide-zeolite catalysts for low-temperature selective catalytic reduction of NOx by ammonia. *Appl. Catal. B Environ.* *291*, 120054. <https://doi.org/10.1016/j.apcatb.2021.120054>.
37. Zhao, S., Luo, C., Tang, B., Chen, L., Xiang, M., Dai, J., Li, H., and Sun, Z. (2022). Research progress on selective catalytic reduction (SCR) catalysts for NO removal from coal-fired flue gas. *Int. J. Surg. Case Rep.* *97*, 107432. <https://doi.org/10.1016/j.fuproc.2022.107432>.
38. Guan, Y., Liu, Y., Lv, Q., Wang, B., and Che, D. (2021). Review on the selective catalytic reduction of NO with H₂ by using novel catalysts. *J. Environ. Chem. Eng.* *9*, 106770. <https://doi.org/10.1016/j.jece.2021.106770>.

39. Kim, H.-S., Kasipandi, S., Kim, J., Kang, S.-H., Kim, J.-H., Ryu, J.-H., and Bae, J.-W. (2020). Current Catalyst Technology of Selective Catalytic Reduction (SCR) for NO_x Removal in South Korea. *Catalysts* 10, 52. <https://doi.org/10.3390/catal10010052>.
40. Wang, Z.y., Guo, R.t., Shi, X., Liu, X.y., Qin, H., Liu, Y.z., Duan, C.p., Guo, D.y., and Pan, W.g. (2020). The superior performance of CoMnO_x catalyst with ball-flowerlike structure for low-temperature selective catalytic reduction of NO_x by NH₃. *Chem. Eng. J.* 381, 122753. <https://doi.org/10.1016/j.cej.2019.122753>.
41. D'Agostino, C., Chansai, S., Gladden, L.F., and Hardacre, C. (2022). Correlating the strength of reducing agent adsorption with Ag/Al₂O₃ catalyst performances in selective catalytic reduction (SCR) of NO_x. *Catal. Today* 384–386, 274–278. <https://doi.org/10.1016/j.cattod.2021.01.013>.
42. Pappas, D.K., Boningari, T., Boolchand, P., and Smirniotis, P.G. (2016). Novel manganese oxide confined interweaved titania nanotubes for the low-temperature Selective Catalytic Reduction (SCR) of NO_x by NH₃. *J. Catal.* 334, 1–13. <https://doi.org/10.1016/j.jcat.2015.11.013>.
43. Guan, B., Zhan, R., Lin, H., and Huang, Z. (2014). Review of state of the art technologies of selective catalytic reduction of NO_x from diesel engine exhaust. *Appl. Therm. Eng.* 66, 395–414. <https://doi.org/10.1016/j.applthermaleng.2014.02.021>.
44. Bartholomew, C.H. (2001). Mechanisms of catalyst deactivation. *Appl. Catal. Gen.* 212, 17–60. [https://doi.org/10.1016/S0926-860X\(00\)00843-7](https://doi.org/10.1016/S0926-860X(00)00843-7).
45. Papageorgaki, S., and Reklaitis, G.V. (1993). Retrofitting a general multipurpose batch chemical plant. *Ind. Eng. Chem. Res.* 32, 345–362. <https://doi.org/10.1021/ie00014a012>.
46. Alves, L., Holz, L.I., Fernandes, C., Ribeirinha, P., Mendes, D., Fagg, D.P., and Mendes, A. (2022). A comprehensive review of NO_x and N₂O mitigation from industrial streams. *Renew. Sustain. Energy Rev.* 155, 111916. <https://doi.org/10.1016/j.rser.2021.111916>.
47. Radojevic, M. (1998). Reduction of nitrogen oxides in flue gases. *Environ. Pollut.* 102, 685–689. [https://doi.org/10.1016/S0269-7491\(98\)80099-7](https://doi.org/10.1016/S0269-7491(98)80099-7).
48. Li, T., Rabuni, M.F., Kleiminger, L., Wang, B., Kelsall, G.H., Hartley, U.W., and Li, K. (2016). A highly-robust solid oxide fuel cell (SOFC): simultaneous greenhouse gas treatment and clean energy generation. *Energy Environ. Sci.* 9, 3682–3686. <https://doi.org/10.1039/C6EE02562E>.
49. Sun, J., Alam, D., Daiyan, R., Masood, H., Zhang, T., Zhou, R., Cullen, P.J., Lovell, E.C., Jalili, A.R., Amal, R., and Amal, R. (2021). A hybrid plasma electrocatalytic process for sustainable ammonia production. *Energy Environ. Sci.* 14, 865–872. <https://doi.org/10.1039/D0EE03769A>.
50. Cherkasov, N., Ibadon, A.O., and Fitzpatrick, P. (2015). A review of the existing and alternative methods for greener nitrogen fixation. *Chem. Eng. Process. Process Intensif.* 90, 24–33. <https://doi.org/10.1016/j.cep.2015.02.004>.
51. Ouyang, B., Zhang, Y., Xia, X., Rawat, R.S., and Fan, H.J. (2018). A brief review on plasma for synthesis and processing of electrode materials. *Mater. Today Nano* 3, 28–47. <https://doi.org/10.1016/j.mtnano.2018.11.002>.
52. Liang, H., Ming, F., and Alshareef, H.N. (2018). Applications of Plasma in Energy Conversion and Storage Materials. *Adv. Energy Mater.* 8, 1801804. <https://doi.org/10.1002/aenm.201801804>.
53. Zhang, Y., Rawat, R.S., and Fan, H.J. (2017). Plasma for Rapid Conversion Reactions and Surface Modification of Electrode Materials. *Small Methods* 1, 1700164. <https://doi.org/10.1002/smt.201700164>.
54. He, C., Wang, J., Fu, L., Zhao, C., and Huo, J. (2022). Associative vs. dissociative mechanism: Electrocatalysis of nitric oxide to ammonia. *Chin. Chem. Lett.* 33, 1051–1057. <https://doi.org/10.1016/j.ccl.2021.09.009>.
55. Niu, H., Zhang, Z., Wang, X., Wan, X., Kuai, C., and Guo, Y. (2021). A Feasible Strategy for Identifying Single-Atom Catalysts Toward Electrochemical NO-to-NH₃ Conversion. *Small* 17, 2102396. <https://doi.org/10.1002/sml.202102396>.
56. Zang, Y., Wu, Q., Wang, S., Huang, B., Dai, Y., and Ma, Y. (2022). High-Throughput Screening of Efficient Biatom Catalysts Based on Monolayer Carbon Nitride for the Nitric Oxide Reduction Reaction. *J. Phys. Chem. Lett.* 13, 527–535. <https://doi.org/10.1021/acs.jpcclett.1c03938>.
57. Liu, S., Xing, G., and Liu, J.y. (2023). Computational screening of single-atom catalysts for direct electrochemical NH₃ synthesis from NO on defective boron phosphide monolayer. *Appl. Surf. Sci.* 611, 155764. <https://doi.org/10.1016/j.apsusc.2022.155764>.
58. Wu, J., and Yu, Y.-X. (2022). A theoretical descriptor for screening efficient NO reduction electrocatalysts from transition-metal atoms on N-doped BP monolayer. *J. Colloid Interface Sci.* 623, 432–444. <https://doi.org/10.1016/j.jcis.2022.05.034>.
59. Shi, P., Pang, D., Zhang, Z., Lin, L., and He, C. (2023). Transition metals embedded Pt (1 0 0) surface as an electrocatalysts for NO reduction reaction: A first-principles study. *Appl. Surf. Sci.* 619, 156744. <https://doi.org/10.1016/j.apsusc.2023.156744>.
60. Tursun, M., and Wu, C. (2022). Single Transition Metal Atoms Anchored on Defective MoS₂ Monolayers for the Electrocatalytic Reduction of Nitric Oxide into Ammonia and Hydroxylamine. *Inorg. Chem.* 61, 17448–17458. <https://doi.org/10.1021/acs.inorgchem.2c02247>.
61. Huang, B., Chen, B., Zhu, G., Peng, J., Zhang, P., Qian, Y., and Li, N. (2022). Electrochemical Ammonia Synthesis via NO Reduction on 2D-MOF. *ChemPhysChem* 23, e202100785. <https://doi.org/10.1002/cphc.202100785>.
62. Lv, X., Mou, T., Li, J., Kou, L., and Frauenheim, T. (2022). Tunable Surface Chemistry in Heterogeneous Bilayer Single-Atom Catalysts for Electrocatalytic NO_x Reduction to Ammonia. *Adv. Funct. Mater.* 32, 2201262. <https://doi.org/10.1002/adfm.202201262>.
63. Zhou, Q., Gong, F., Xie, Y., Xia, D., Hu, Z., Wang, S., Liu, L., and Xiao, Z. (2022). A general strategy for designing metal-free catalysts for highly-efficient nitric oxide reduction to ammonia. *Fuel* 310, 122442. <https://doi.org/10.1016/j.fuel.2021.122442>.
64. He, C., Yang, H., Xi, M., Fu, L., Huo, J., and Zhao, C. (2022). Efficient electrocatalytic reduction of NO to ammonia on BC₃ nanosheets. *Environ. Res.* 212, 113479. <https://doi.org/10.1016/j.envres.2022.113479>.
65. Zhao, S., Li, Y., Guo, Z., Tang, C., Sa, B., Miao, N., Zhou, J., and Sun, Z. (2022). Breaking scaling relations in nitric oxide reduction by surface functionalization of MXenes. *J. Mater. Chem.* 10, 25201–25211. <https://doi.org/10.1039/D2TA06354A>.
66. Amrillah, T., Supandi, A.R., Puspasari, V., Hermawan, A., and Seh, Z.W. (2022). MXene-Based Photocatalysts and Electrocatalysts for CO₂ Conversion to Chemicals. *Trans. Tianjin Univ.* 28, 307–322. <https://doi.org/10.1007/s12209-022-00328-9>.
67. Zhao, Y., Zheng, L., Jiang, D., Xia, W., Xu, X., Yamauchi, Y., Ge, J., and Tang, J. (2021). Nanoengineering Metal–Organic Framework–Based Materials for Use in Electrochemical CO₂ Reduction Reactions. *Small* 17, 20065900–e2006618. <https://doi.org/10.1002/sml.202006590>.
68. Wang, Y., Wang, D., and Li, Y. (2021). Rational Design of Single-Atom Site Electrocatalysts: From Theoretical Understandings to Practical Applications. *Adv. Mater.* 33, 2008151. <https://doi.org/10.1002/adma.202008151>.
69. Qiao, B., Wang, A., Yang, X., Allard, L.F., Jiang, Z., Cui, Y., Liu, J., Li, J., and Zhang, T. (2011). Single-atom catalysis of CO oxidation using Pt₁/FeO_x. *Nat. Chem.* 3, 634–641. <https://doi.org/10.1038/nchem.1095>.
70. Su, J., Ge, R., Dong, Y., Hao, F., and Chen, L. (2018). Recent progress in single-atom electrocatalysts: concept, synthesis, and applications in clean energy conversion. *J. Mater. Chem.* 6, 14025–14042. <https://doi.org/10.1039/C8TA04064H>.
71. Peng, X., Mi, Y., Bao, H., Liu, Y., Qi, D., Qiu, Y., Zhuo, L., Zhao, S., Sun, J., Tang, X., et al. (2020). Ambient electrosynthesis of ammonia with efficient denitration. *Nano Energy* 78, 105321. <https://doi.org/10.1016/j.nanoen.2020.105321>.

72. Chen, K., Zhang, G., Li, X., Zhao, X., and Chu, K. (2022). Electrochemical NO reduction to NH₃ on Cu single atom catalyst. *Nano Res.* **16**, 5857–5863. <https://doi.org/10.1007/s12274-023-5384-9>.
73. Chen, L., Sun, W., Xu, Z., Hao, M., Li, B., Liu, X., Ma, J., Wang, L., Li, C., and Wang, W. (2022). Ultrafine Cu nanoparticles decorated porous TiO₂ for high-efficient electrocatalytic reduction of NO to synthesize NH₃. *Ceram. Int.* **48**, 21151–21161. <https://doi.org/10.1016/j.ceramint.2022.04.006>.
74. Choi, J., Du, H.-L., Nguyen, C.K., Suryanto, B.H.R., Simonov, A.N., and MacFarlane, D.R. (2020). Electroreduction of Nitrates, Nitrites, and Gaseous Nitrogen Oxides: A Potential Source of Ammonia in Dinitrogen Reduction Studies. *ACS Energy Lett.* **5**, 2095–2097. <https://doi.org/10.1021/acscenergylett.0c00924>.
75. Liu, Q., Lin, Y., Yue, L., Liang, J., Zhang, L., Li, T., Luo, Y., Liu, M., You, J., Alshehri, A.A., et al. (2022). Bi nanoparticles/carbon nanosheet composite: A high-efficiency electrocatalyst for NO reduction to NH₃. *Nano Res.* **15**, 5032–5037. <https://doi.org/10.1007/s12274-022-4283-9>.
76. Li, X., Chen, K., Lu, X., Ma, D., and Chu, K. (2023). Atomically dispersed Co catalyst for electrocatalytic NO reduction to NH₃. *Chem. Eng. J.* **454**, 140333. <https://doi.org/10.1016/j.cej.2022.140333>.
77. Chen, K., Wang, J., Zhang, H., Ma, D., and Chu, K. (2023). Self-Tandem Electrocatalytic NO Reduction to NH₃ on a W Single-Atom Catalyst. *Nano Lett.* **23**, 1735–1742. <https://doi.org/10.1021/acsnanolett.2c04444>.
78. Chen, K., Zhang, Y., Xiang, J., Zhao, X., Li, X., and Chu, K. (2023). p-Block Antimony Single-Atom Catalysts for Nitric Oxide Electroreduction to Ammonia. *ACS Energy Lett.* **8**, 1281–1288. <https://doi.org/10.1021/acscenergylett.2c02882>.
79. Chen, K., Wang, G., Guo, Y., Ma, D., and Chu, K. (2023). Iridium single-atom catalyst for highly efficient NO electroreduction to NH₃. *Nano Res.* <https://doi.org/10.1007/s12274-023-5556-7>.
80. Chen, K., Zhang, N., Wang, F., Kang, J., and Chu, K. (2023). Main-group indium single-atom catalysts for electrocatalytic NO reduction to NH₃. *J. Mater. Chem.* **11**, 6814–6819. <https://doi.org/10.1039/D3TA00606A>.
81. Chen, K., Zhang, Y., Du, W., Guo, Y., and Chu, K. (2023). Atomically isolated and unsaturated Sb sites created on Sb₂S₃ for highly selective NO electroreduction to NH₃. *Inorg. Chem. Front.* **10**, 2708–2715. <https://doi.org/10.1039/D3QI00268C>.
82. Hermawan, A., Septiani, N.L.W., Taufik, A., Yulianto, B., Suyatman, and Yin, S. (2021). Advanced Strategies to Improve Performances of Molybdenum-Based Gas Sensors. *Nano-Micro Lett.* **13**, 207. <https://doi.org/10.1007/s40820-021-00724-1>.
83. Manzeli, S., Ovchinnikov, D., Pasquier, D., Yazyev, O.V., and Kis, A. (2017). 2D transition metal dichalcogenides. *Nat. Rev. Mater.* **2**, 17033. <https://doi.org/10.1038/natrevmats.2017.33>.
84. Tursun, M., and Wu, C. (2021). NO Electroreduction by Transition Metal Dichalcogenides with Chalcogen Vacancies. *Chemelectrochem* **8**, 3113–3122. <https://doi.org/10.1002/celec.202100790>.
85. Chen, K., Shen, P., Zhang, N., Ma, D., and Chu, K. (2023). Electrocatalytic NO Reduction to NH₃ on Mo₂C Nanosheets. *Inorg. Chem.* **62**, 653–658. <https://doi.org/10.1021/acs.inorgchem.2c03714>.
86. Ouyang, L., Zhou, Q., Liang, J., Zhang, L., Yue, L., Li, Z., Li, J., Luo, Y., Liu, Q., Li, N., et al. (2022). High-efficiency NO electroreduction to NH₃ over honeycomb carbon nanofiber at ambient conditions. *J. Colloid Interface Sci.* **616**, 261–267. <https://doi.org/10.1016/j.jcis.2022.02.074>.
87. Liang, J., Liu, P., Li, Q., Li, T., Yue, L., Luo, Y., Liu, Q., Li, N., Tang, B., Alshehri, A.A., et al. (2022). Amorphous Boron Carbide on Titanium Dioxide Nanobelt Arrays for High-Efficiency Electrocatalytic NO Reduction to NH₃. *Angew Chem. Int. Ed. Engl.* **61**, 2022020877–e202202095. <https://doi.org/10.1002/anie.202202087>.
88. Sharif, H.M.A., Li, T., Mahmood, N., Ahmad, M., Xu, J., Mahmood, A., Djellabi, R., and Yang, B. (2021). Thermally activated epoxy-functionalized carbon as an electrocatalyst for efficient NO_x reduction. *Carbon N. Y.* **182**, 516–524. <https://doi.org/10.1016/j.carbon.2021.06.042>.
89. Krzywdka, P.M., Paradelo Rodríguez, A., Benes, N.E., Mei, B.T., and Mul, G. (2022). Effect of Electrolyte and Electrode Configuration on Cu-Catalyzed Nitric Oxide Reduction to Ammonia. *Chemelectrochem* **9**, 1–7. <https://doi.org/10.1002/celec.202101273>.
90. Shi, J., Wang, C., Yang, R., Chen, F., Meng, N., Yu, Y., and Zhang, B. (2021). Promoting nitric oxide electroreduction to ammonia over electron-rich Cu modulated by Ru doping. *Sci. China Chem.* **64**, 1493–1497. <https://doi.org/10.1007/s11426-021-1073-5>.
91. Zhang, H., Li, Y., Cheng, C., Zhou, J., Yin, P., Wu, H., Liang, Z., Zhang, J., Yun, Q., Wang, A.L., et al. (2023). Isolated Electron-Rich Ruthenium Atoms in Intermetallic Compounds for Boosting Electrochemical Nitric Oxide Reduction to Ammonia. *Angew Chem. Int. Ed. Engl.* **62**, e202213351. <https://doi.org/10.1002/anie.202213351>.
92. Lin, Y., Liang, J., Li, H., Zhang, L., Mou, T., Li, T., Yue, L., Ji, Y., Liu, Q., Luo, Y., et al. (2022). Bi nanodendrites for highly efficient electrocatalytic NO reduction to NH₃ at ambient conditions. *Mater. Today Phys.* **22**, 100611. <https://doi.org/10.1016/j.mtphys.2022.100611>.
93. Ko, B.H., Hasa, B., Shin, H., Zhao, Y., and Jiao, F. (2022). Electrochemical Reduction of Gaseous Nitrogen Oxides on Transition Metals at Ambient Conditions. *J. Am. Chem. Soc.* **144**, 1258–1266. <https://doi.org/10.1021/jacs.1c10535>.
94. Li, X., Gao, Y., Li, Y., Li, Y., Liu, H., Yang, Z., Wu, H., and Hu, Y. (2022). Electrocatalytic Reduction of Low-Concentration Nitric Oxide into Ammonia over Ru Nanosheets. *ACS Energy Lett.* **300**, 1187–1195. <https://doi.org/10.1021/acscenergylett.2c00207>.
95. Wei, T., Bao, H., Wang, X., Zhang, S., Liu, Q., Luo, J., and Liu, X. (2023). Ionic Liquid-Assisted Electrocatalytic NO Reduction to NH₃ by P-Doped MoS₂. *ChemCatChem* **15**. <https://doi.org/10.1002/cctc.202201411>.
96. Chen, K., Wang, J., Kang, J., Lu, X., Zhao, X., and Chu, K. (2023). Atomically Fe-doped MoS₂-x with Fe-Mo dual sites for efficient electrocatalytic NO reduction to NH₃. *Appl. Catal. B Environ.* **324**, 122241. <https://doi.org/10.1016/j.apcatb.2022.122241>.
97. Li, K., Shi, Z., Wang, L., Wang, W., Liu, Y., Cheng, H., Yang, Y., and Zhang, L. (2023). Efficient electrochemical NO reduction to NH₃ over metal-free g-C₃N₄ nanosheets and the role of interface microenvironment. *J. Hazard Mater.* **448**, 130890. <https://doi.org/10.1016/j.jhazmat.2023.130890>.
98. Liu, P., Liang, J., Wang, J., Zhang, L., Li, J., Yue, L., Ren, Y., Li, T., Luo, Y., Li, N., et al. (2021). High-performance NH₃ production via NO electroreduction over a NiO nanosheet array. *Chem. Commun.* **57**, 13562–13565. <https://doi.org/10.1039/D1CC06113E>.
99. Liang, J., Chen, H., Mou, T., Zhang, L., Lin, Y., Yue, L., Luo, Y., Liu, Q., Li, N., Alshehri, A.A., et al. (2022). Coupling denitrification and ammonia synthesis via selective electrochemical reduction of nitric oxide over Fe₂O₃ nanorods. *J. Mater. Chem.* **10**, 6454–6462. <https://doi.org/10.1039/D2TA00744D>.
100. Zhang, S., Liu, Q., Tang, X., Zhou, Z., Fan, T., You, Y., Zhang, Q., Zhang, S., Luo, J., and Liu, X. (2023). Electrocatalytic reduction of NO to NH₃ in ionic liquids by P-doped TiO₂ nanotubes. *Front. Chem. Sci. Eng.* **17**, 726–734. <https://doi.org/10.1007/s11705-022-2274-8>.
101. Li, X., Xing, W., Hu, T., Luo, K., Wang, J., and Tang, W. (2022). Recent advances in transition-metal phosphide electrocatalysts: Synthetic approach, improvement strategies and environmental applications. *Coord. Chem. Rev.* **473**, 214811. <https://doi.org/10.1016/j.ccr.2022.214811>.
102. Pu, Z., Liu, T., Amini, I.S., Cheng, R., Wang, P., Zhang, C., Ji, P., Hu, W., Liu, J., and Mu, S. (2020). Transition-Metal Phosphides: Activity Origin, Energy-Related Electrocatalysis Applications, and Synthetic Strategies. *Adv. Funct. Mater.* **30**, 2004009. <https://doi.org/10.1002/adfm.202004009>.
103. Shi, Y., Li, M., Yu, Y., and Zhang, B. (2020). Recent advances in nanostructured transition metal phosphides: synthesis and energy-related applications. *Energy Environ. Sci.* **13**, 4564–4582. <https://doi.org/10.1039/D0EE02577A>.

104. Zhang, H., Wang, G., Wang, C., Liu, Y., Yang, Y., Wang, C., Jiang, W., Fu, L., and Xu, J. (2022). CoP nanowires on carbon cloth for electrocatalytic NO_x-reduction to ammonia. *J. Electroanal. Chem.* 910, 116171. <https://doi.org/10.1016/j.jelechem.2022.116171>.
105. Mou, T., Liang, J., Ma, Z., Zhang, L., Lin, Y., Li, T., Liu, Q., Luo, Y., Liu, Y., Gao, S., et al. (2021). High-efficiency electrohydrogenation of nitric oxide to ammonia on a Ni₂P nanoarray under ambient conditions. *J. Mater. Chem.* 9, 24268–24275. <https://doi.org/10.1039/D1TA07455E>.
106. Zhang, G., Wan, Y., Zhao, H., Guo, Y., and Chu, K. (2023). A metal-free catalyst for electrocatalytic NO reduction to NH₃. *Dalton Trans.* 52, 6248–6253. <https://doi.org/10.1039/D3DT00994G>.
107. Zhang, L., Zhou, Q., Liang, J., Yue, L., Li, T., Luo, Y., Liu, Q., Li, N., Tang, B., Gong, F., et al. (2022). Enhancing Electrocatalytic NO Reduction to NH₃ by the CoS Nanosheet with Sulfur Vacancies. *Inorg. Chem.* 61, 8096–8102. <https://doi.org/10.1021/acs.inorgchem.2c01112>.
108. Li, Z., Zhou, Q., Liang, J., Zhang, L., Fan, X., Zhao, D., Cai, Z., Li, J., Zheng, D., He, X., et al. (2023). Defective TiO_{2-x} for High-Performance Electrocatalytic NO Reduction toward Ambient NH₃ Production. *Small* 19, 2300291. <https://doi.org/10.1002/smll.202300291>.
109. Li, X., Zhang, G., Shen, P., Zhao, X., and Chu, K. (2023). A defect engineered p-block SnS_{2-x} catalyst for efficient electrocatalytic NO reduction to NH₃. *Inorg. Chem. Front.* 10, 280–287. <https://doi.org/10.1039/D2QI02118H>.
110. Meng, G., Jin, M., Wei, T., Liu, Q., Zhang, S., Peng, X., Luo, J., and Liu, X. (2022). MoC nanocrystals confined in N-doped carbon nanosheets toward highly selective electrocatalytic nitric oxide reduction to ammonia. *Nano Res.* 15, 8890–8896. <https://doi.org/10.1007/s12274-022-4747-y>.
111. Qi, D., Lv, F., Wei, T., Jin, M., Meng, G., Zhang, S., Liu, Q., Liu, W., Ma, D., Hamdy, M.S., et al. (2022). High-efficiency electrocatalytic NO reduction to NH₃ by nanoporous VN. *Nano Res. Energy* 1, e9120022. <https://doi.org/10.26599/NRE.2022.9120022>.
112. Chen, K., Tian, Y., Li, Y., Liu, Y., and Chu, K. (2023). Amorphous NiB₂ for electroreduction of NO to NH₃. *J. Mater. Chem.* 11, 7409–7414. <https://doi.org/10.1039/D3TA00394A>.
113. Kim, D., Shin, D., Heo, J., Lim, H., Lim, J.A., Jeong, H.M., Kim, B.S., Heo, I., Oh, I., Lee, B., et al. (2020). Unveiling Electrode-Electrolyte Design-Based NO Reduction for NH₃Synthesis. *ACS Energy Lett.* 5, 3647–3656. <https://doi.org/10.1021/acscenergylett.0c02082>.
114. De Vooy, A.C.A., Beltramo, G.L., Van Riet, B., Van Veen, J.A.R., and Koper, M.T.M. (2004). Mechanisms of electrochemical reduction and oxidation of nitric oxide. *Electrochim. Acta* 49, 1307–1314. <https://doi.org/10.1016/j.electacta.2003.07.020>.
115. Rabiee, H., Ge, L., Zhang, X., Hu, S., Li, M., and Yuan, Z. (2021). Gas diffusion electrodes (GDEs) for electrochemical reduction of carbon dioxide, carbon monoxide, and dinitrogen to value-added products: a review. *Energy Environ. Sci.* 14, 1959–2008. <https://doi.org/10.1039/D0EE03756G>.
116. Cheon, S., Kim, W.J., Kim, D.Y., Kwon, Y., and Han, J.-I. (2022). Electro-synthesis of Ammonia from Dilute Nitric Oxide on a Gas Diffusion Electrode. *ACS Energy Lett.* 7, 958–965. <https://doi.org/10.1021/acscenergylett.1c02552>.
117. Meng, G., Wei, T., Liu, W., Li, W., Zhang, S., Liu, W., Liu, Q., Bao, H., Luo, J., and Liu, X. (2022). NiFe layered double hydroxide nanosheet array for high-efficiency electrocatalytic reduction of nitric oxide to ammonia. *Chem. Commun.* 58, 8097–8100. <https://doi.org/10.1039/D2CC02463B>.
118. Zhang, W., Qin, X., Wei, T., Liu, Q., Luo, J., and Liu, X. (2023). Single atomic cerium sites anchored on nitrogen-doped hollow carbon spheres for highly selective electroreduction of nitric oxide to ammonia. *J. Colloid Interface Sci.* 638, 650–657. <https://doi.org/10.1016/j.jcis.2023.02.026>.
119. Liang, J., Hu, W.-F., Song, B., Mou, T., Zhang, L., Luo, Y., Liu, Q., Alshehri, A.A., Hamdy, M.S., Yang, L.-M., and Sun, X. (2022). Efficient nitric oxide electroreduction toward ambient ammonia synthesis catalyzed by a CoP nanoarray. *Inorg. Chem. Front.* 9, 1366–1372. <https://doi.org/10.1039/D2QI00002D>.
120. Wang, D., Chen, Z.-W., Gu, K., Chen, C., Liu, Y., Wei, X., Singh, C.V., and Wang, S. (2023). Hexagonal Cobalt Nanosheets for High-Performance Electrocatalytic NO Reduction to NH₃. *J. Am. Chem. Soc.* 145, 6899–6904. <https://doi.org/10.1021/jacs.3c00276>.